UNIVERSIDADE DE SÃO PAULO
INSTITUTO DE FÍSICA DE SÃO CARLOS

Michelle Alejandra Moreno Armijos

Construction of an experiment providing cold strontium atoms for atomic interferometry in a ring cavity

São Carlos

2020

Michelle Alejandra Moreno Armijos

Construction of an experiment providing cold strontium atoms for atomic interferometry in a ring cavity

Dissertation presented to the Graduate Program in Physics at the Instituto de Física de São Carlos, Universidade de São Paulo, to obtain the degree of Master in Science.

Concentration area: Applied Physics

Supervisor: Prof. Dr. Philippe W. Courteille

Original version

São Carlos

2020

Moreno Armijos, Michelle Alejandra
Construction of an experiment providing cold strontium atoms for atomic interferometry in a ring cavity / Michelle Alejandra Moreno Armijos; advisor Philippe W. Courteille -- São Carlos 2020.
68 p.

Dissertation (Master's degree - Graduate Program in Applied Physics) -- Instituto de Física de São Carlos, Universidade de São Paulo - Brasil , 2020.

1. Cold atoms . 2. Strontium. 3. Magneto-optical trap. 4. Saturated absorption spectroscopy. I. Courteille, Philippe W., advisor. II. Title.

To my grandmother Rosario.

ACKNOWLEDGEMENTS

I want to express my deepest thanks to the fellowship and friendship of all the people who accompanied me on this journey. Thank you very much to all of you.

My supervisor Dr. Philippe Courteille, first for the opportunitty to work in his laboratory and for his enthusiasm for the project, for his support, encouragement and patience. I also want to thank Dr. Hans Keßler with whom I worked the first year of the master's degree and who taught me from scratch everything necessary to work in the laboratory, thanks for your demand, patience and support.

I also want to thank the professors of Universidade Federal de São Carlos UFSCAR, Rodrigo Shiozaki and Raul Celestrino Teixeira, who are part of our research group and always gave us the knowledge, guided and supported the development of this project.

I thank my fellow labmates in Strontium group: Pablo, Pedro, Marcia, Lucas and especially I thank the wonderful scientists Camila and Dalila with whom we led and worked hardly on this project. Thank you all for your friendship.

My biggest thanks to my family for all the support you have shown me through this research, the culmination of two years of learning. To my parents, Carlos and Isabel for being my fundamental pillar and for having supported me unconditionally, despite the adversities and inconveniences that arose. I am grateful to my boyfriend Andrés, you never stopped teaching me something new, either about physics or how to try overcome difficulties and enjoy life.

I would like to express my sincere gratitude to the Universidade de São Paulo and the thanks to CAPES and FAPESP for the financial support. Thanks to all national agencies and institutions which entrust the Brazilian's resources to national and foreign researchers to develop science and technology in Brazil.

This study was financed in part by the Coordenação de Aperfeiçoamento de Pessoal de Nível Superior – Brasil (CAPES) – Finance Code 001

ABSTRACT

MORENO ARMIJOS, M. A. **Construction of an experiment providing cold strontium atoms for atomic interferometry in a ring cavity**. 2020. 68p. Dissertação (Mestrado em Ciências) - Instituto de Física de São Carlos, Universidade de São Paulo, São Carlos, 2020.

This thesis describes the first steps to fulfill the main objective of our project: the development of a gravimetry system based on the continuous monitoring of Bloch oscillations performed by ultra-cold strontium atoms. The realization of this project comprises three main stages: the first stage consists in obtaining a magneto-optical trap in the broad transition of 461 nm of strontium, the second stage is the transfer to a magneto-optical trap in the narrow intercombination line of 689 nm, and finally the third stage is the monitoring of Bloch oscillations of the cloud of atoms in a ring cavity. This work details the first stage of the project, the creation of an experimental apparatus which produces ultra-cold strontium atoms in the transition of 461 nm, as well as the characterization of the cloud of atoms, temperature, size, number of atoms, etc. For this project, a new experimental apparatus has been designed and realized. It involves an ultra-high vacuum system, magnetic field sources, laser systems and optical instruments which are required for cooling, trapping and repumping strontium atoms. A novel feature is the implementation of a transversely loaded two-dimensional magneto-optical trap, which serves as a source of a cold strontium atomic beam. A loading rate of the atomic beam into a nearby three-dimensional magneto-optical trap exceeding 10^5 s^{-1} for the ^{88}Sr isotope at a moderate dispenser temperature of 600 °C are reported. The temperature of the cloud is about 4 mK and its size 0.3 mm, these characteristics suggest that the state of the atomic trap is in optimal conditions to make the transfer to the optical magneto trap in the intercombination line and thus continue with the second stage of the project.

Keywords: Cold atoms. Strontium. Magneto-optical trap. Saturated absorption spectroscopy.

RESUMO

MORENO ARMIJOS, M. A. **Construção de um experimento que fornece átomos frios de estrôncio para interferometria atômica em uma cavidade anelar**. 2020. 68p. Dissertação (Mestrado em Ciências) - Instituto de Física de São Carlos, Universidade de São Paulo, São Carlos, 2020.

Este trabalho descreve os primeiros passos para cumprir o objetivo principal do nosso projeto: o desenvolvimento de um sistema de gravimetria baseado no monitoramento contínuo das oscilações de Bloch realizadas por átomos de estrôncio ultrafrios. A realização deste projeto compreende três etapas principais: a primeira consiste em obter uma armadilha magneto-óptica na transição de 461 nm do estrôncio; a segunda etapa é a transferência para uma armadilha magneto-óptica na estreita linha de intercombinação de 689 nm e, finalmente, o terceiro estágio é o monitoramento das oscilações de Bloch da nuvem de átomos em uma cavidade anelar. Este trabalho detalha a primeira etapa do projeto, a criação de um aparelho experimental que produz átomos de estrôncio ultrafrios na transição de 461 nm, bem como a caracterização da nuvem de átomos, temperatura, tamanho, forma e número de átomos. Para esta pesquisa, um novo aparelho experimental foi projetado e realizado. Compreende um sistema de vácuo ultra alto, fontes de campo magnético, sistemas de laser e instrumentos ópticos necessários para resfriar, aprisionar e rebombear átomos de estrôncio. Uma característica nova é a implementação de uma armadilha magneto-óptica bidimensional carregada transversalmente, que serve como fonte de um feixe atômico de estrôncio frio. Uma taxa de carregamento do feixe atômico em uma armadilha magneto-óptica tridimensional próxima que excede 10^5 s^{-1} para o isótopo ^{88} Sr a uma temperatura moderada do dispenser de 600 °C é reportado. A temperatura da nuvem é de cerca de 4 mK e seu tamanho é de 0.3 mm, essas características sugerem que o estado da armadilha atômica está em condições ideais para fazer a transferência para a armadilha magnética óptica na linha de intercombinação e, assim, continuar com o segunda etapa do projeto.

Palavras-chave: Átomos frios. Estrôncio. Armadilha magneto-óptica. Espectroscopia de absorção saturada.

LIST OF FIGURES

LIST OF TABLES

CONTENTS

1 INTRODUCTION

1.1 Outline of the thesis

This thesis is divided into three main chapters organized as follows:
The first chapter presents a brief description of the properties and structure of strontium energy levels and the main cooling transitions. Chapter (2) summarizes the theoretical foundations of laser cooling and trapping: light forces, temperature limits and magneto-optical trapping of strontium. Chapter (3) presents a detailed description of the experiment, the vacuum system, pre-cooling stage, science chamber, saturation spectroscopy, imaging method and an analysis to determine the optimal parameters of the system and characterizes the number of atoms, optical density, and temperature of the cloud, which are of vital importance for the next step of the project: obtaining a magneto-optical trap in the intercombination line of strontium.

1.2 Gravitational quantum sensing with atoms

Gravimeters measure the Earth's local gravitational field. Classical absolute gravimeters work by measuring the vertical acceleration of mass in vacuum. However, their precision, is limited. Gravimeters based on atomic interferometry are able to detect very small gravitational anomalies which arise due to oil reserves,[1] mineral deposits, lava flow,[2] etc. being desirable in many industries the development of compact and portable devices. Atomic interferometry is equally important in fundamental research, where they are used for measurements of fundamental constants,[3, 4] and the precise measurements of Casimir forces.[5, 6] In order to perform a sensitive force measurement, a long time of coherent evolution of the atomic wave function is required. The most common effects limiting the coherence time for ultracold atoms are perturbations due to electromagnetic fields and atom-atom interactions. The most abundant strontium isotope ^{88}Sr is in this respect a good choice because in the ground state it has zero orbital, spin, and nuclear angular momentum, which makes it insensitive to electric and magnetic fields. In addition, ^{88}Sr has small atom-atom interactions;[7] this has so far hindered the achievement of Bose-Einstein condensation for this atom.[8] However, Killian and Mickelson in 2010 achieved BEC of ^{88}Sr via sympathetic cooling with ^{87}Sr.[9] The small interactions become an important feature in experiments where collisions lead to a loss of coherence limiting the measurement time and the potential sensitivity.

Our research project has the aim to verify whether Bloch oscillations of ultracold atoms confined in a vertical standing light wave created by light fields inside a laser-pumped optical ring cavity can be monitored non-destructively. In this way, it would be

possible to overcome the destructive nature of the measurement where the results are reconstructed by varying the evolution time. In atomic gravimeters a new technique that allows monitoring of the Bloch oscillations in vivo has been proposed.[10, 11] A constant external force driving the Bloch dynamics in systems of ultracold atoms can be provided by either a constant acceleration of the confining potential or by a real force, in this case gravity. As a result, the atoms undergo Bloch oscillations with a frequency proportional to gravitational acceleration and to the wavelength of the laser generating the standing wave. The former possibility was used in the first experiment on Bloch oscillations with cold atoms.[12]

Most imaging techniques monitor the trajectory of an atomic cloud by taking snapshots at different stages of its evolution via single shots of incident probe light. Unfortunately, the radiation pressure exerted by the probe light destroys the coherence of the matter wave, because the light is scattered in all directions, as well as the atoms receiving the photonic recoil. The measurement process can be improved if instead of making successive images of the atomic motion, the impact of the atomic displacement on the confining standing light wave is monitored. Indeed, recent experiments have shown that atoms moving in a stationary light wave can modify the amplitude or phase of the light, assuming that the wave is sufficiently decoupled from the driving laser beams, this phenomenon is called Collective atomic recoil laser (CARL).[13, 14] The dynamics has been experimentally demonstrated in[15, 16] using a ring cavity. The role of the cavity is to amplify the interaction between the atoms and laser light (see Fig. (1)). If one of two counter-propagating cavity modes is pumped by a sufficiently far-detuned laser, the cloud of atoms could only respond by scattering light into the backward direction. Now, the scattering process turns coherent, the mechanical impact of the incident light becomes predictable and can be taken into account, while heating can be avoided. Then our major goal is to make sure that the proposed non-destructive technique of monitoring the atomic Bloch oscillations via their backaction on the cavity fields allows to gather information on the periodicity of the Bloch oscillations faster than other conventional techniques.[7, 17, 18] If this process can be sped up considerably, a better signal-to-noise ratio can be obtained in shorter integration times, which means, in a given time higher precision can be reached for the determination of the gravitational acceleration.

It is important to emphasize that the goal of our experiment is not to construct a better gravimeter, but to provide a proof that continuous operation of an atomic gravimeter is technically feasible and could be a realistic way to improve its performance.[19, 20]

1.3 Strontium

Strontium is part of the alkaline earth atoms located in Group 2 of the periodic table. The presence of a second valence electron in alkaline earth atoms creates a rich

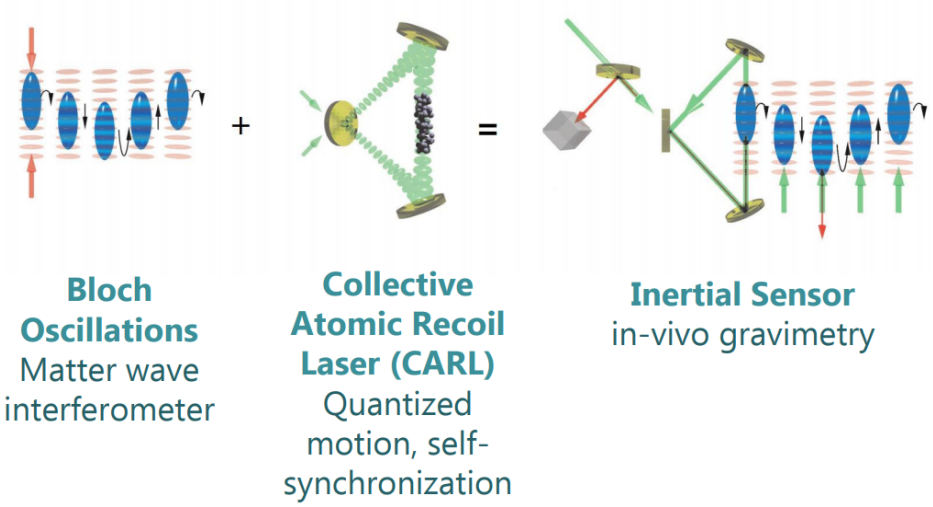

Figure 1 – Scheme of the proposed inertial sensor based on the continuous detection of Bloch oscillations of atoms falling inside a vertical light wave sustained by a ring cavity.

Source: By the author.

mixture of electronic states, neatly divided into spin singlet (intrinsic electronic spin S=0) and spin triplet (S=1) states. There are four naturally occurring isotopes of strontium, one of them is fermionic: ^{87}Sr, and three are bosonic: ^{84}Sr, ^{86}Sr, ^{88}Sr. Being ^{88}Sr the most abundant strontium isotope in nature (82.58 %). The nuclear spin of all bosonic alkaline earth elements is zero, which prevents the appearance of a hyperfine structure and are therefore not sensitive to stray magnetic fields. The work on this experiment is focused on the most abundant isotope ^{88}Sr The isotopes and their properties are found in Tab. (1).

Table 1 – Natural abundance, mass, nuclear spin and scattering length of the four stable strontium isotopes.

isotope	abundance	mass (u)	nuclear spin	scattering length
^{88}Sr	82.58 %	87.906	0	-2 a_0
^{87}Sr	7.00 %	86.909	9/2	
^{86}Sr	9.86 %	85.909	0	+800 a_0
^{84}Sr	0.56 %	83.913	0	+123 a_0

Source: Adapted from SORRETINO;[21] STELLMER.[22]

The main advantage of strontium is that most of the required wavelengths are in the visible or near infrared range, with all of them being directly accessible by diode lasers. This greatly reduces the complexity of the setup, which is favorable for a mobile experiment. Due to the antiparallel alignment of the two valence electron spins, the electron spin and the electronic magnetic dipole moment of the singlet $^1S_0$ state are zero ($J = 0$). Because of this, there are no magnetic Feshbach resonances[22, 23] and the sensitivity to

magnetic fields are significantly reduced, which is an advantage for applications in precision measurements.[24, 25]

1.4 Level structure and cooling transitions of strontium

The energy level term diagram for strontium is shown in Fig. (2). Strong dipole allowed transitions exist from the ground state to higher lying $^1P_1$ states. For strontium and several other alkaline earth atoms the very first excited state is a triplet state ^3P, with allowed dipole transitions to a variety of ^3S and ^3D states. Due to the dipole selection rule $\Delta S = 0$, no dipole transitions are allowed between the spin singlet and spin triplet states. If we assume pure L-S coupling, the three 5s5p ^3P states are forbidden to decay to the ground state, and are therefore meta-stable. However, the spin-orbit interaction provides a finite lifetime for the $^3P_1$ state, allowing weak electric dipole transitions to take place. This narrow transition is called an intercombination transition and comprises much of the current interest in alkaline earth atoms.

The atomic structure in strontium allows for two main cooling transitions, see Fig. (2). One is the $^1S_0 - ^1P_1$ transition is strong and the lowest $^1P_1$ state has only very weak decay rates to states other than $^1S_0$. The corresponding wavelength is 461 nm with a broad linewidth of $\Gamma/2\pi = 30.5$ MHz. This transition is well-suited for traditional laser cooling, permitting a thermal beam of dilute Sr gas to be cooled to mK temperatures and collected in a magneto optical trap. The second main cooling transition is particularly interesting because of its very fine intercombination, the transition $^1S_0 - ^3P_1$ of $\Gamma/2\pi = 7.6$ kHz linewidth in 689 nm.This will allow the investigation of the interaction of the atoms with the macroscopic ring cavity in this regime. But the greatest advantage of this fine transition lies in the fact that it allows to reach ultra low temperatures by purely optical cooling, we avoid to apply evaporative cooling methods, which traditionally are slow and always come with important losses of atoms.

Strontium atoms need to be ultracold to be contained within an optical lattice. Atoms cooled below 1μK can be achieved using a 3D magneto optical trap (MOT) on the very narrow linewidth transition.[28] Strontium, however, has a low vapour pressure so it must be heated to ~ 600 K to achieve a sufficient flux of atoms.[22] The velocity distribution of the atoms follows the Maxwell-Boltzmann distribution so few atoms will have low enough velocity to be captured by a 3D MOT. The atoms, therefore, must be pre-cooled and this is typically done using a Zeeman slower. However, in this experiment, we will instead use a 2D MOT which traps the atoms in two dimensions creating a collimated atomic beam along the remaining axis. More experimental details will be explained on chapter (3).

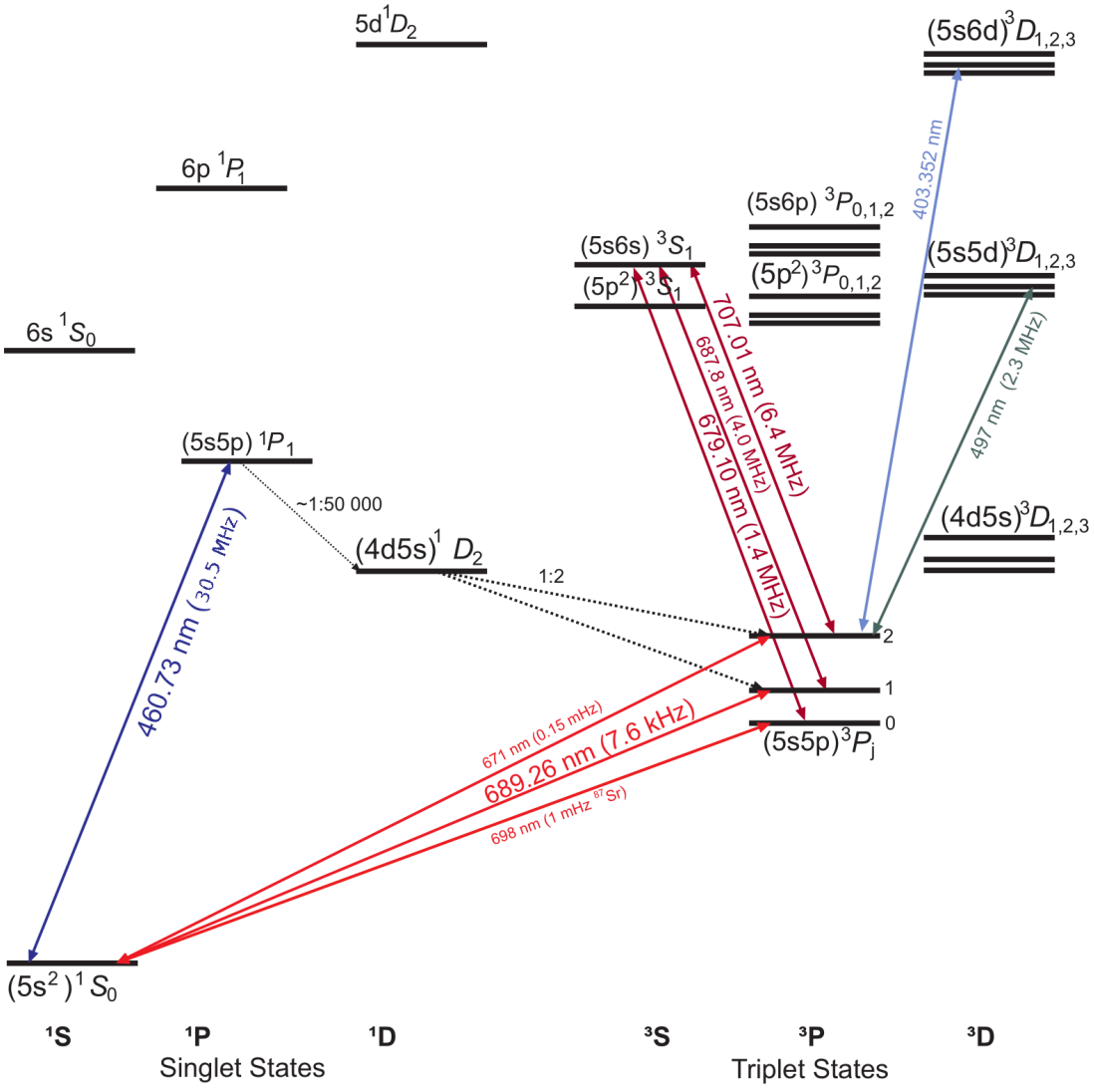

Figure 2 – Selection of the level scheme of strontium. Simplified energy level diagram for ^{88}Sr showing the two main cooling transitions at 461 nm and 689 nm, the radiative decay channels for the $^1P_1$ excited state, and the relevant repumping scheme. The energy levels are described in the usual Russell Saunders notation of $^{2S+1}L_J$

Source: Adapted from: KOCK;[26] BARKER.[27]

2 LASER COOLING AND TRAPPING: THEORETICAL FOUNDATION

2.1 Laser cooling and trapping

2.1.1 Light forces

To compute the forces of light on an atom, we describe the atom as a two-level system: A fundamental level $|1\rangle$ and an excited level $|2\rangle$ decaying to the fundamental level with the rate Γ. The energy difference between the levels is $\hbar\omega_0 \equiv E_2 - E_1$. The light with frequency ω is derived from a laser beam, which can be detuned from the atomic transition, $\Delta \equiv \omega - \omega_0$. To describe the interaction, we consider the part of the total Hamiltonian describing the interaction[29]

$$\hat{H} = \hbar\omega\hat{a}^\dagger\hat{a} + \hat{H}_{int} + \hat{H}_{atm} \quad \text{where} \quad \hat{H}_{int} = \hbar\Omega(\hat{\mathbf{r}})\, e^{i\mathbf{k}\hat{\mathbf{r}}}\, \hat{a}^\dagger\hat{\sigma} + c.c., \tag{2.1}$$

where $\hat{\sigma} \equiv |g\rangle\langle e|$ and $\hat{a} \equiv \Sigma_n |n\rangle\langle n+1|$ and $\hbar\Omega(\hat{\mathbf{r}}) \equiv \mathbf{d}\ .\ \mathbf{E}$ is the coupling constant or Rabi frequency. The Rabi frequency is the radian frequency of the Rabi cycle undergone for a given atomic transition in a given light field.

Using the density operator $\hat{\rho}$, and letting the atom be at the position r = 0, it is possible to calculate the force that light exerts on the atom

$$\mathbf{F}(\mathbf{0}) = -\frac{1}{2}\hbar \bigtriangledown_{\mathbf{r}} \Omega(\mathbf{0})(\rho_{12}e^{-i\Delta t} + \rho_{21}e^{i\Delta t}) - \frac{i}{2}\hbar\mathbf{k}\Omega(\mathbf{0})(\rho_{12}e^{-i\Delta t} - \rho_{21}e^{i\Delta t}). \tag{2.2}$$

The quantities $\rho_{12} = \rho_{21}^*$ are the coherences, which develop in a two-level system excited by a laser beam. Inserting the stationary solutions of Bloch equations (ρ_{22} and ρ_{12}) and the definition of the cross section $\sigma_a(\Delta) = \sigma_{a0}\frac{\Gamma^2}{4\Delta^2+2\Omega^2+\Gamma^2}$

$$\rho_{22} = \frac{(2\Delta - i\Gamma)\Omega}{4\Delta^2 + 2\Omega^2 + \Gamma^2} \quad \text{and} \quad \rho_{12} = \frac{\Omega^2}{4\Delta^2 + 2\Omega^2 + \Gamma^2}e^{-i\Delta t}, \tag{2.3}$$

where Δ is the detuning between the laser frequency and the resonance frequency $\Delta = \omega_l - \omega_0$, Γ is the spontaneous decay rate, and Ω is the Rabi frequency. The force that light exerts on the atom can be written as:

$$\mathbf{F}(\mathbf{0}) = -\frac{1}{2}\hbar\Delta \bigtriangledown_{\mathbf{r}} \ln\left(1 + \frac{2\Omega^2}{4\Delta^2 + \Gamma^2}\right) + \hbar\mathbf{k}\frac{\Omega^2}{\Gamma}\frac{\sigma_a(\Delta)}{\sigma_{a0}}, \tag{2.4}$$

where the resonant cross section for a classical transition is $\sigma_{a0} = 3\lambda^2/2\pi$.

From Eq. (2.4), the light force has two contributions. The dipolar gradient force and the radiation pressure. The ***dipolar force*** can be derived from a potential (conservative

force). It can be interpreted as resulting from absorption processes immediately followed by self-stimulated emission. Near resonance it is dispersive, far from resonance it can be approximated by,

$$\mathbf{F}_{dp} = \bigtriangledown_{\mathbf{r}} \frac{-\hbar\Delta\Omega^2}{4\Delta^2+\Gamma^2} \overset{|\Delta|\gg\Gamma}{\rightarrow} -\bigtriangledown_{\mathbf{r}} \frac{\hbar\Omega^2}{4\Delta}. \tag{2.5}$$

For example, a standing wave is composed of two counterpropagating laser beams, their interference produces an amplitude gradient that is not present in a traveling wave. For $\Delta < 0$ the force drives atoms to positions where the intensity has a maximum, whereas $\Delta > 0$ the atoms are attracted to the intensity minima.

The ***radiation pressure force*** results from the absorption followed by spontaneous emission. This force is dissipative and close to resonance it is absorbing. It is proportional to the intensity gradient and saturates at large intensity. With $\Omega^2 = \sigma_{a_0}\Gamma I/\hbar\omega$ we get the formula,

$$\mathbf{F}_{rp} = \hbar\mathbf{k}\frac{I}{\hbar\omega}\sigma_a(\Delta) = \hbar\mathbf{k}\gamma_{sct}, \tag{2.6}$$

which describes the force as a product of the number of photons in the incident beam $I/\hbar\omega$, the absorption cross section $\sigma_a(\Delta)$ and the recoil momentum per photon $\hbar k$. γ_{sct} is the scattering rate ($\gamma_{sct} = \Gamma\rho_{22}$). Increasing the rate of absorption by increasing the intensity does not increase the force without limit, since that would only increase the rate of stimulated emission, where the transfer of momentum is opposite in direction compared to the absorption. Thus the force saturates to a maximum value of $\hbar k\Gamma/2$, because ρ_{22} has a maximum value of $1/2$. Radiation pressure vanishes for an atom at rest in a standing wave. Atoms can absorb light from either of the two counter-propagating beams that make up the standing wave and the average momentum transfer then vanishes.

2.1.2 Laser cooling via the Doppler shift

The Doppler broadening is simply the apparent frequency distribution of a sample of radiating atoms at temperature T. The contribution of each atom to the radiation appears detuned by the Doppler shift because of its velocity.

In Fig. (3) a two-level atom is moving at a velocity v opposite to the propagation of the light beam. The first order Doppler shift $-\mathbf{v}\cdot\mathbf{k}$, is proportional to the projection of velocity on the line of sight.[30] The atom is out of resonance if the light frequency is tuned to the resonant frequency, it is $\omega = \omega_0$. However, photons can be absorbed in the resonance if the Doppler shift is compensated by detuning to a lower frequency $\omega = \omega_0 - kv$. For each photon the atom absorbs, it acquires an amount $\hbar k$ of linear momentum opposite to its initial momentum. Then the light is remitted as spontaneous emission in a random direction, and on average the total momentum is zero.

The average emission frequency of the atoms is ω_0, since the Doppler broadened spectrum is centered on the rest frame resonance frequency. Therefore, the average atom radiates more energy than it absorbs after absorbing a photon with a frequency in the red side of the resonance. This is the basis of Doppler cooling, energy and momentum decreased and the atoms cool.[31]

If we consider an atom propagating in $+z$ direction with the velocity v_z counter-propagating to a light wave with detuning Δ, the total detuning considering the Doppler effect will be $\Delta \to \Delta + kv_z$. The force $\mathbf{F}_-$ acting on the atom will be in the opposite direction to the motion. In general the force is,

$$\mathbf{F}_\pm = \pm\hbar\mathbf{k}\Gamma\frac{\Omega^2}{4(\Delta \mp kv_z)^2 + 2\Omega^2 + \Gamma^2}. \tag{2.7}$$

Supposing that we have two light fields propagating in directions $\pm z$, the total force will be $\mathbf{F} = \mathbf{F}_+ + \mathbf{F}_-$. If kv_z is small compared to Γ and Δ, we find through a Taylor expansion

$$F_z \simeq \hbar k s\frac{kv_z(2\Delta/\Gamma)}{(4\Delta^2 + 2\Omega^2 + \Gamma^2)^2}. \tag{2.8}$$

Fig. (3) shows this restoring dissipative force as a function of v_z at a detuning $\Delta = -\Gamma$ with $I = I_{sat}/2$.

The expression Eq. (2.8) shows that, for positive detuning, it accelerates atoms traveling in the $+z$ direction and decelerates atoms traveling in the $-z$ direction. For any given velocity v, if the detuning is fixed at $\Delta = k|v|$, the force is far more effective at deceleration than at acceleration. This is because an atom copropagating with the light at velocity v sees a detuning of $\Delta = -2k|v|$ due to the Doppler effect. As illustrated in Fig. (4), with red detuning, the atoms experience a greatly reduced force compared to the atoms propagating toward the light source which is in resonance. For negative detuning, the forces reverse.

However, the atom will not cool down indefinitely. At some point, the Doppler cooling rate will be balanced by the heating rate coming from the momentum fluctuations of the atom absorbing and remitting photons.

2.1.3 Magneto-optical trapping

In order to cool atoms effectively using the Doppler effect, it is necessary to achieve a net cooling of atoms along either direction of the Cartesian axis. For this purpose, pairs of counter-propagating laser beams are needed in all three axes. The red-detuned beams can interact with the atoms traveling in positive or negative direction along any given axis. The cold atoms must be collected in a central region, on the other hand, atoms away from the center should experience Doppler cooling and a net force driving them to the center.

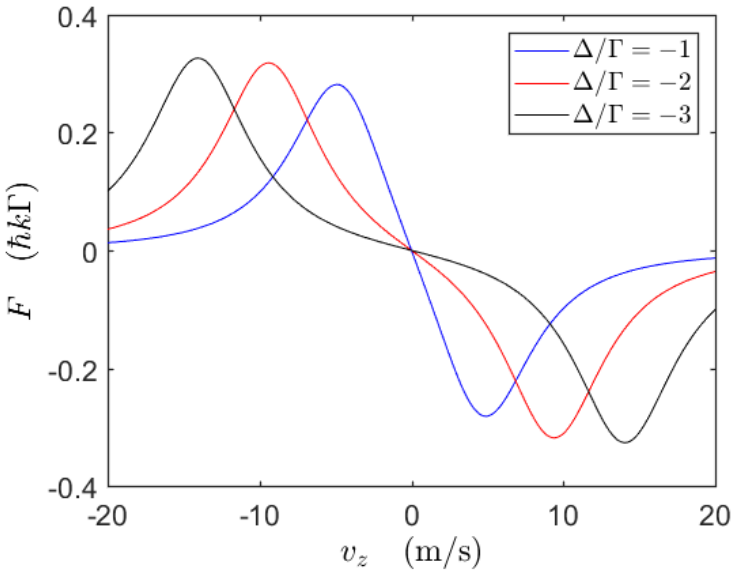

Figure 3 – Doppler force due to one-dimensional radiative pressure as a function of atomic velocity along the z-axis for red detuning Δ/Γ = -1, -2, -3 at a light intensity of $I = I_{sat}/2$. At low velocities, the force on an atom varies linearly with velocity. At high velocities, the force begins to decrease, and atoms with velocities outside the linear region are said to be outside the capture range. As we change the detuning of the laser, we can see that the slope of the force changes. The linear restoring force as a function of velocity is necessary for cooling to work, since the goal of this system is to drive the atoms toward low velocity.

Source: By the author.

The key ingredient of a magneto-optical trap (hereafter MOT), is the introduction of a magnetic field gradient that increases linearly from the origin. Due to linear Zeeman splitting, states with opposite magnetic projections on either side of the origin experience a magnetic restoring force that point to the center of the trap, as shown in Fig. (5a). The restoring force acts only on atoms that reach the excited state with after the interaction with one of the red-detuned beams and producing a magnetic moment. Once the standing waves slowed and cooled the atoms in each axis, it is possible for them to fall and accumulate into the central capture region (where the magnetic field is zero) if their velocity is low enough.

The operating principle of a MOT is shown in Fig. (5a) for a simple 1D case with a $J = 0$ to $J = 1$ transition, for the three-dimensional case the principle is the same, a typically used scheme is depicted in Fig. (5b). For an external magnetic field $B(z) = b\ z$ $(b > 0)$, the resulting Zeeman shift of the m_J sub-levels is

$$\frac{\Delta E}{\hbar} = \frac{\mu_B g_F m_F}{\hbar} \frac{\mathrm{d}B}{\mathrm{d}z} z \equiv z \partial_z \omega_{zeem} \tag{2.9}$$

It is also part of a MOT the counterpropagating laser beams along the directions $\pm z$ with

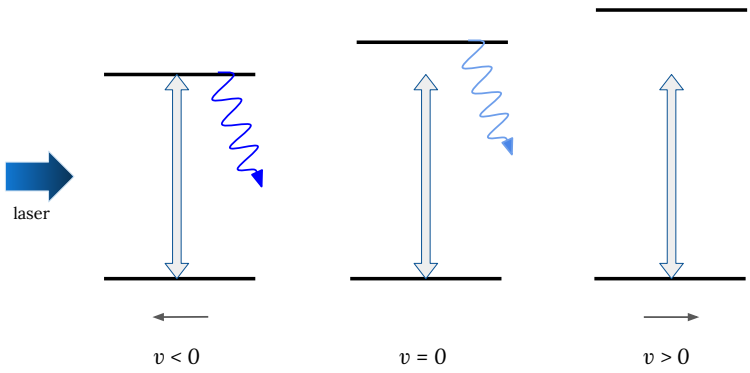

Figure 4 – Illustration of the Doppler-shift due to atomic motion. To the atom moving toward the right side, the laser's wavelength will appear shorter, which means its frequency is higher. This change to a higher frequency is called blueshift. However, if the atom is on the moving toward the left, then the opposite will happen, this change to a lower frequency is called redshift.

Source: By the author.

circular polarizations of opposite signs and tuned to the red of the atomic transition. From Fig. (5a) an atom moving in $\pm z$ direction will scatter $\sigma^{\pm}$ type photons at a faster rate than $\sigma^{\pm}$ type photons, because the Zeeman effect will pull the $\Delta m_J = \mp 1$ transition closer to the laser frequency. The expression for the radiation pressure force extends Eq. (2.7) to include the Doppler effect kv_z and the Zeeman effect,

$$F_{\pm z} = -\hbar k \Gamma \frac{\Omega^2}{4(\Delta \pm k v_z \pm z \partial_z \omega_{zeem})^2 + 2\Omega^2 + \Gamma^2}. \tag{2.10}$$

The detuning that results in an extremum of the cooling rate can be calculated by $\partial \langle F \rangle / \partial \Delta = 0$, it is possible to estimate the optimal detuning by setting

$$\frac{\partial}{\partial \Delta} \left(\frac{\Delta}{(\Gamma^2 + \Delta^2)^2} \right) = 0 \tag{2.11}$$

The result is $\Delta = (\Gamma/\sqrt{3}) \approx \Gamma/2$, this relation suggests that temperature limit of the Doppler cooling is set by the energy balance between cooling and heating at this detuning, the lowest temperature due to the Doppler limit is therefore

$$k_B T_D = \frac{1}{2} \hbar \Gamma. \tag{2.12}$$

2.2 Blue MOT of strontium

Recently, alkaline earth atoms have been investigated by only a few atom-optics research groups, mainly due to the more challenging wavelengths required for laser cooling

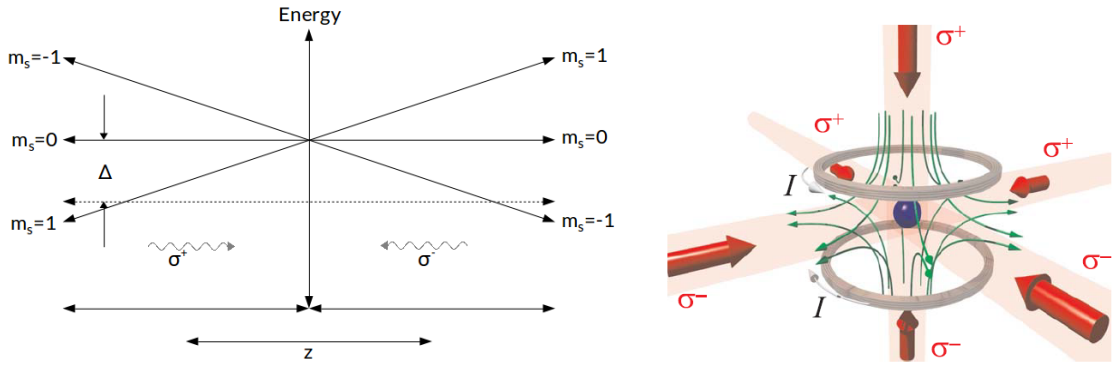

(a) (b)

Figure 5 – (a) One-dimensional MOT combining Doppler cooling with a magnetic restoring force centered on the origin. (b) Schematic of a three-dimensional MOT composed by six counter propagating beams with opposite circular polarizarion and two coils in anti-Helmholtz configuration creating a quadrupole magnetic field.

Source: Adapted from METCALF.[31]

and trapping. But the two electron level structure being at the origin of the greater laser requirements, also offers a more versatile platform for experimental studies as in case of strontium.

The blue MOT provides the initial confinement and cooling of atomic strontium gases in the experiment. It is a six-beam magneto-optical trap operating on the broad ($\Gamma = 2\pi 30.5$ MHz), $^1S_0 - ^1P_1$ transition at 461 nm. Due to the absence of hyperfine structure of the $^1S_0$ state and the broad transition linewidth, the behavior of the blue MOT can be described by Doppler-cooling theory.[27]

2.2.1 Optical repumping

Due to the presence of the low lying $^1D_2$ state, the singlet cooling transition is not completely closed as shows Fig. (2). The decay path from $^1P_1$, which eventually leads to atoms being shelved into the $^3P_2$ state. This loss mechanism limits the total atom number in the blue MOT, as the MOT lifetime (in seconds) can be estimated given the decay rates as[32]

$$\tau = 1.56 \times 10^{-3} \left(1 + \frac{1 + 4(\Delta/\Gamma)^2}{I/I_{sat}}\right) s, \tag{2.13}$$

where s is the saturation parameter, defined as:

$$s \equiv \frac{2|\Omega|^2}{4\Delta^2 + \Gamma^2}, \tag{2.14}$$

it measures the degree of saturation of a transition, it can also be defined the on-resonance saturation parameter as $I/I_{sat} = 2\Omega^2/\Gamma^2$. For the trapping beam parameters described

above, the saturation parameter s is typically 0.5, and the MOT lifetime is around 20 ms. This short lifetime will limit the number of atoms loaded into the MOT, and it could be improved by optical repumping. In our case, to repump the 5s5p $^3P_2$ atoms to the 5s^2 $^1S_0$ state, we drive the 5s5p $^3P_2 - 5s6s\ ^3S_1$ transition by a laser at 707 nm, the selection rules permit that from here they can decay to any of the 5s5p ^3P states. If they decay to the 5s5p $^3P_2$ state they are again pumped to the 5s6s $^3S_1$ state. If they decay to the 5s5p $^3P_1$ state they can decay to the ground state. And if they decay to the 5s5p $^3P_0$ state, which is a very long lived state, a second repumping laser at 679 nm is required to pump them again to the 5s6s $^3S_1$ state. This scheme was chosen for our experiment since we have available laser diodes for both wavelengths.

Table 2 – Laser cooling parameters for the two main cooling transitions of strontium, including the saturation intensity, Doppler and recoil temperatures.

Transition	$\Gamma/2\pi$	λ (nm)	I_{sat}	$T_{Doppler}$	T_{recoil}
5s^2 $^1S_0 - 5s5p\ ^1P_1$	30.5 MHz	461	43 mW/cm^2	720 μK	1.02 μK
5s^2 $^1S_0 - 5s5p\ ^3P_1$	7.6 kHz	689	3 mW/cm^2	180 nK	460 nK

Source: Adapted from BOYD;[33] STELLMER.[22]

3 LASER COOLING OF NEUTRAL STRONTIUM ATOMS: EXPERIMENTAL APPARATUS

We use a Ti:sapphire laser and a frequency doubler (MSquared, SolsTiS and ECD-X) to generate the blue laser light for the cooling transition at 461 nm. The Ti:Sapphire laser is pumped by 15.25 W of lightpower of a diode-pumped solid-state laser (Sprout-G Lighthouse Photonics) at 532 nm in the TEM_{00} mode. The Ti:sapphire laser provides 1.3 W. of light power at 922 nm. After the frequency doubler, the laser system typically delivers a power of 600 mW at 461 nm. For frequency monitoring, the Ti:sapphire laser at 922 nm is coupled to a high-accuracy wavelength-meter (High Finesse, WSU 30 t) via a single-mode fiber.

The blue laser output is coupled to an optical path system consisting of acousto-optic modulators (AOM), polarizing beam splitters (PBS), waveplates, and fiber couplers to deliver all the laser frequencies and powers involved in the experiment, such as the saturation spectroscopy, 2D MOT and 3D MOT cooling beams, the probe beam (used for imaging), etc. see Fig. (6). Each part of the blue system will be described throughout this chapter.

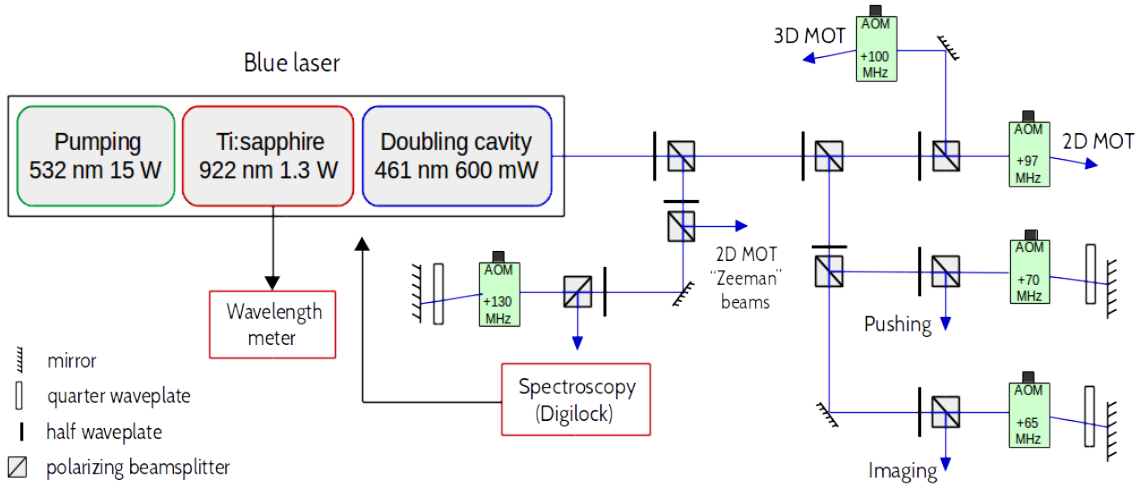

Figure 6 – Blue system experiment setup. The 600 mW of blue light coming out of the doubling cavity is divided into six beams: saturation spectroscopy, "Zeeman" beam, pushing beam, imaging beam, 2D MOT and 3D MOT whose frequency is established using AOMs (except for "Zeeman" beam). Part of the infrared light of the Ti:Sapphire is used to monitor the frequency of the laser in a wavelength meter.

Source: By the author.

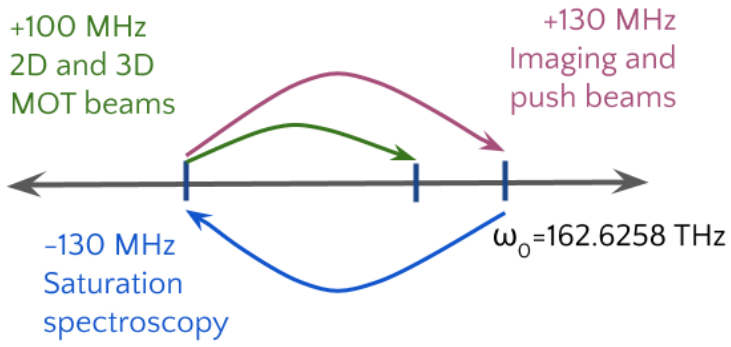

Figure 7 – AOMs frequency of each beam used in the blue setup respect to the resonance frequency ω_0. Initially, the blue laser is locked at the strontium resonance frequency, then we use saturation spectroscopy to shift -130 MHz and lock at this frequency. The frequency of the 2D and 3D MOT beams are shifted +100 MHz (leaving them red-detuned towards the resonance). Finally, the frequency of the push and imaging beams are shifted +130 MHz and are on resonance.

Source: By the author.

3.1 Saturated absorption spectroscopy

In order to stabilize the laser at the desired frequency, it needs to be locked to an external frequency reference via an electronic feedback. In our experiment, the feedback is provided by the commercial Toptica DigiLock system. The frequency reference is obtained via standard saturated absorption spectroscopy.

Saturation spectroscopy is based on the velocity-selective saturation of molecular transitions with Doppler broadening. By using this technique, the spectral resolution is no longer limited by the Doppler width of the 600 K hot gas stored in a heated vacuum cell, but only by the narrower width of the Lamb dip,[34] which is essentially the natural linewidth with a little increase due to (homogeneous) pressure broadening.

The standard method to resolve such a narrow transition embedded in a broad background is to use the technique of saturated absorption spectroscopy. The basic idea is shown schematically in Fig. (10). In addition to the probe beam, there is a much stronger pump beam that counter-propagates with respect to the probe, and plays the role of saturating the transition. Since the probability of transition is nonlinear in the light intensity,[35] the probe shows decreased absorption when the pump is also resonant with the same transition. By counter-propagating the two beams, we ensure that the two beams are simultaneously resonant with zero velocity atoms. The consequence of this on the probe spectrum is shown in Fig. (12). The absorption of the probe beam in the absence of the pump shows a broad curve, but a narrow dip appears at when the pump is turned on.

The atomic density can be derived by applying the equation of state of a classical ideal gas

$$n(T) = \frac{p(T)}{k_B T}. \tag{3.1}$$

The thermal Maxwell-Boltzmann distribution of an ideal gas is given by

$$P(v) = \sqrt{\frac{2}{\pi}\left(\frac{m}{k_B T}\right)^3}\, v^2\, \mathrm{e}^{-\frac{mv^2}{2k_B T}}, \tag{3.2}$$

and this is illustrated in Fig (8). To know the speed of the atoms inside the cell, it is necessary to know the vapor pressure of strontium (see Fig. (9)) at a certain temperature. In our case, the minimum pressure we achieve is in the order of 10^{-3} mbar, and according to Fig. (9) temperature of the oven should reach 700 K (427 °C).

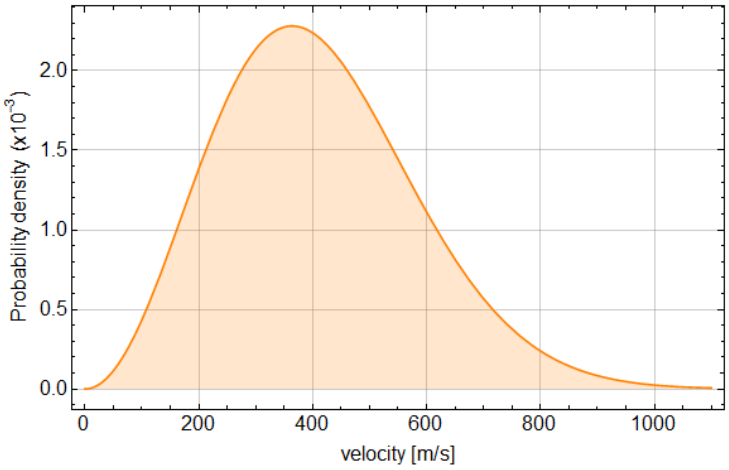

Figure 8 – Maxwell Boltzmann velocity distribution of an ideal strontium gas at 700 K.

Source: By the author.

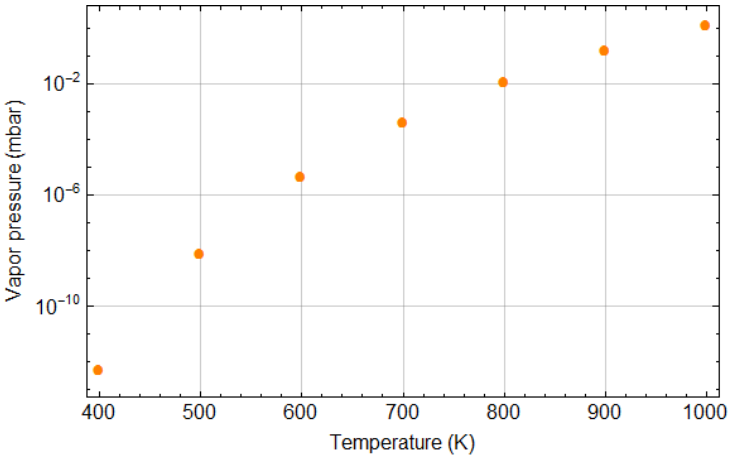

Figure 9 – Strontium vapor pressure versus temperature.

Source: Adapted from LIDE.[36]

Using these values, we estimated the most probable velocity $\hat{v}$ and mean velocity $\bar{v}$ of the atoms:

$$\hat{v} = \sqrt{\frac{2k_BT}{m}} \quad \bar{v} = \sqrt{\frac{8k_BT}{\pi m}} \tag{3.3}$$

which gives $\bar{v} = 410.6$ m/s at a temperature of 700 K. An important aspect that should be verified when designed the cell is the transit broadening (Fourier-limited resolution caused by a finite atom-light interaction time). For a linewidth of 30.5 MHz (lifetime $t = 5$ ns) the traveled distance in the excited state results in $d_{exc} = \bar{v}\ t \approx 2\ \mu$m. This small distance will not have any effect of transit broadening and we can neglect it. This is advantageous because we can use a beam with a small diameter (approximately 2 mm) and it is not necessary to allocate too much laser power to the spectroscopy system.

3.1.1 Mounting the spectroscopy cell

Our spectroscopy cell consists mainly of a tube of 300 mm length and 19 mm/16 mm outer/inner diameter, with an oven attached to its center. The oven has an inner/outer diameter of 26mm/30mm and extends 45mm from the main axis of the tube to its bottom, plus 6mm for an extra thick wall where a thermocouple is attached for monitoring the temperature in the oven. At the ends of the tube there are two MDC CF16 viewports with anti-reflection coating. To control the pressure, another tube was soldered perpendicularly to the main tube and connected via a CF16 flange to another T at which a Pirani gauge was attached to measure the pressure.

To create the vacuum conditions, we rapidly filled the oven with small chunks of strontium to avoid the strontium starts oxidizing during this process. Then we closed the viewports using CF16 copper gaskets. As a buffer gas we used argon, which we fed under constant flux into the cell. We pumped and baked at 100 °C for one day to evaporate all impurities. Finally, after pumping the spectroscopy cell stayed with 2×10^{-3} mbar.

In order to heat the cell, an isolated resistor wire was wrapped around the oven, the total resistance is 23 Ω. Around the fixed resistor we wrapped several layers of a plain fiberglass tape and finally we wrapped a layer of aluminum foil to thermally isolate the cell.

Once we finished the construction and pumping of the cell, we closed all the valves and measured a pressure of 10^{-3} mbar. Then, we slowly increased the current until the cell reached a temperature of $\sim$ 400 °C. Under these conditions we observed a strong fluorescence once the beam has passed through the windows. As the light absorption was very high and the power of our beam is limited to 12 mW, we lowered the cell temperature to 320 °C (with 1.3 A of current) so that the absorption is less and the probe beam crosses the windows and reaches the photodetector.

3.1.2 Spectroscopy setup

Our experimental setup for saturation spectroscopy is illustrated in Fig. (10). The output beam from a laser is split into a strong pump beam (saturation beam) and a weak probe beam, which pass through the absorbing sample in opposite directions. A picture of the final assembly is in Fig. (11). When the transmitted probe beam signal is measured as a function of the laser frequency, the detection signal shows the absorption profiles with Doppler broadening, and in addition shows a Lamb dip at the center of the absorption line.

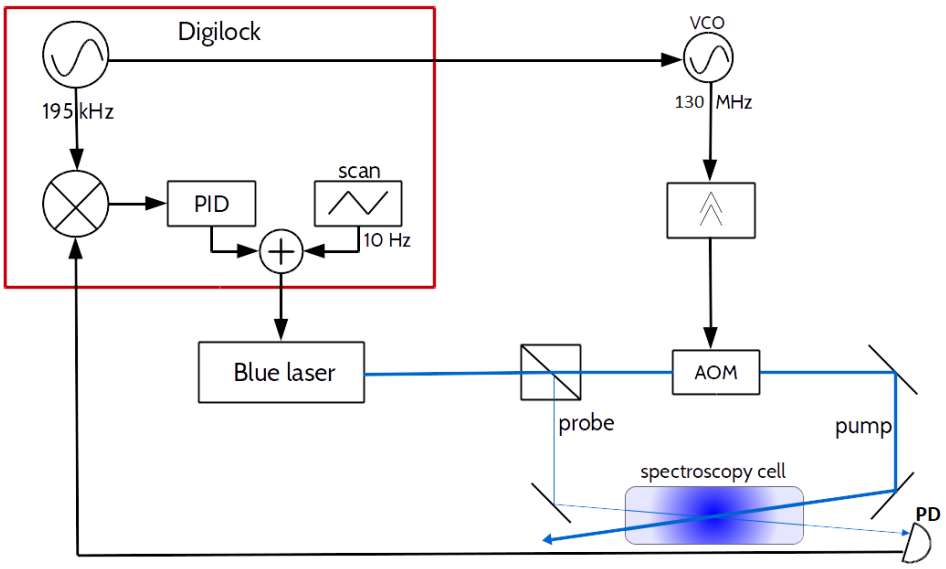

Figure 10 – Doppler free saturation spectroscopy setup. The blue light is divided into probe and pump beams, the frequency of the pump beam is run by a double-pass AOM by 260 MHz. After the beams pass through the cell, the probe beam reaches a photodetector (PD) and it sends the signal to Digilock. Using a Digilock system the light is modulated with a frequency of 195 kHz and the absorption signal is scanned with a 10 Hz ramp. Together with a PID and a lock-in system, the blue laser frequency is locked in the peak of the Lamb dip.

Source: By the author.

For conducting saturation spectroscopy on the $^1S_0 \rightarrow {}^1P_1$ line of strontium, we take into account some specific properties of strontium, such as the vapor pressure which demand high temperatures, or the window coating properties, which demand a setup that protects the windows.

In the experiment we use 3 mW of blue light for probe beam and 7 mW for pump beam, the $1/e^2$ radius is 2.4 mm and frequency is shifted using an AOM by 130 MHz. The spectroscopy cell has a temperature of 320 °C. Fig. (12) shows a typical spectroscopy signal obtained.

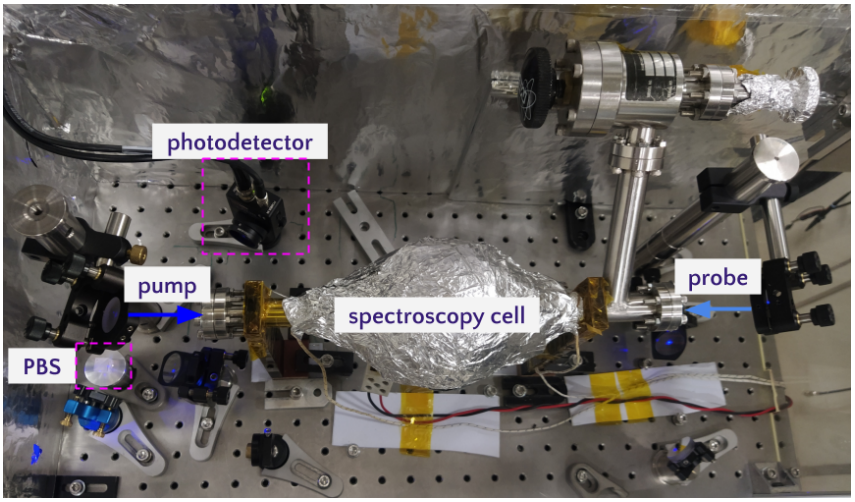

Figure 11 – Final assembly of the Doppler free saturation spectroscopy setup. The pump and probe beams pass through the two viewports of the spectroscopy cell and are absorbed by the strontium gas inside. After crossing the cell, both beams reach a polarized beam splitter (PBS) which separates them and directs the probe beam towards a photodetector.

Source: By the author.

3.2 Description of the 2D MOT setup

A 2D MOT combines two principles to cool and trap atoms in two dimensions: lasers use Doppler cooling to reduce the atomic temperature to near 20 mK thus cooling them and a spatially dependent magnetic field modulates the light forces acting on the atoms, creating a restoring force towards the zero of the magnetic field that traps them.

Atoms cooled to below 10 mK can be achieved using a 3D MOT on the blue transition.[37, 38] Strontium, however, has a low vapour pressure so it must be heated to $\sim$ 600 K to achieve a sufficient flux of atoms. The velocity distribution of the atoms follows the Maxwell-Boltzmann distribution so few atoms will have low enough velocity to be captured by a 3D MOT.[39] The atoms, therefore must be pre-cooled, and this is typically done using a Zeeman slower. In this experiment we will instead use a 2D MOT which traps the atoms in two dimensions creating a collimated atomic beam along the remaining axis. Once the atoms are trapped, the atomic beam can be transferred to a 3D MOT by using a push beam.

The use of a 2D MOT offers two main advantages over a Zeeman slower. The heated atom source, in our case a dispenser, can be installed in such a way that it has no direct line of sight with the trapped atoms, reducing the amount of black body radiation emitted from the heated dispenser that the atoms experience. Black body radiation is currently one of the main errors contributing to the error budget of strontium clocks.[38, 40] Estimations show that the 2D MOT can have a similar atom flux as Zeeman slowers.[41, 42]

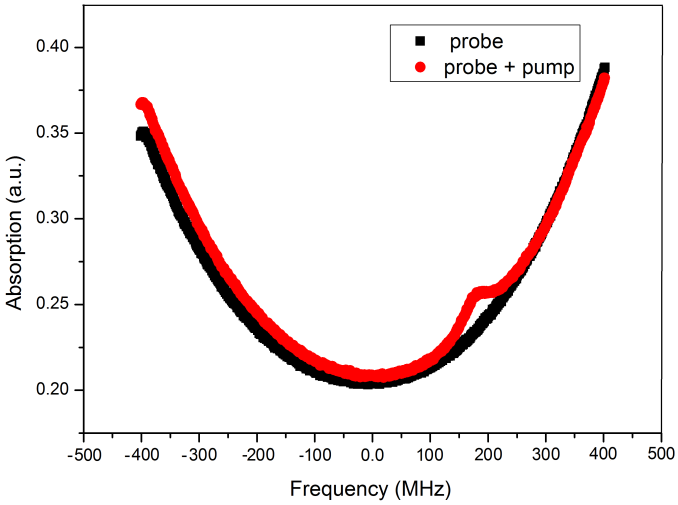

Figure 12 – Absorption signal of strontium blue transition with pump saturating beam where a Lamb dip is exhibited (red) and without the pump beam (black).

Source: By the author.

The 2D MOT of strontium was achieved on the blue cooling transition $(5s^2)^1\mathrm{S}_0 - (5s5p)^1\mathrm{P}_1$, which has a wavelength of 461 nm and linewidth of $\Gamma = 2\pi \times 30.5$ MHz.

3.2.1 Vacuum chamber

The vacuum system consists of two sections, the 2D MOT chamber and the science chamber or 3D MOT chamber as shown in Fig. (13). Valves were placed between each stage to prevent contamination of the entire system during pumping and bake-out process. A differential pressure is implemented between the 2D and 3D MOT chambers. To prevent background atoms knocking strontium atoms out of the trap, the pressure in the 3D MOT should be as low as possible. The 2D MOT requires a high flux of atoms to create the atomic beam. This increases the pressure within the 2D MOT. The two vacuum chambers are linked by a 2 cm long differential vacuum tube with 2 mm inner diameter. Combinations of ion pumps and non-evaporable getter pumps allows us to maintain a vacuum of 10^{-8} mbar in the 2D MOT chamber and 10^{-10} mbar in the 3D MOT chamber. The distance between the centers of the 2D MOT chamber and the science chamber is approximately 20 cm.

The 2D MOT is loaded from a strontium dispenser (AlfaVakuo e.U.) run at a current of 6.5 A, the temperature of the oven is about 600 °C. Buffles are mounted around the dispenser with viewports obstructing simple atomic trajectories in order to avoid the strontium to stick to the walls and windows of the chamber.

The chamber is formed from several individual pieces which had been bathed in an

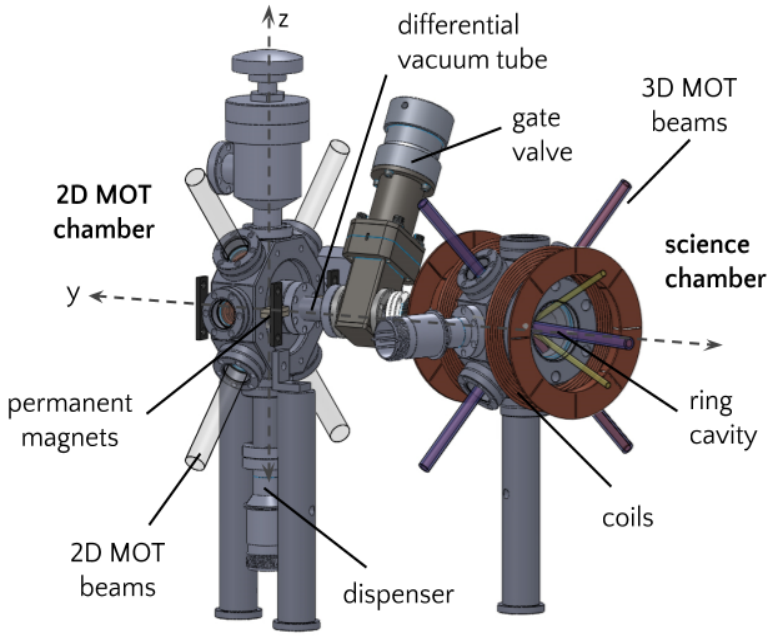

Figure 13 – Scheme of 2D MOT and science chamber. The 2D MOT chamber has six viewports, the beams pass through four of them (in retroreflected configuration) and through other viewport the push beam crosses (not shown in the figure) along the y axis. The remaining viewport is used for monitoring the atomic cloud. Between the 2D and 3D cameras there is a differential vacuum tube and connects them. The 3D MOT camera has an arrangement of two coils and through the viewports they cross six counterpropaganting beams. In the center of the chamber is located the ring cavity.

Source: By the author.

ultrasonic bath of acetone and alcohol before their assembly to remove their impurities. All pieces were attached to each other via ConFlat type vacuum flanges. Rough, turbo and ionic pumps were then used to pump the system for the duration of the experiment.

3.2.2 Magnetic Field

The 2D MOT is operated with permanent magnets arranged in a way, such that the symmetry axis is magnetic field free. To calculate the magnetic field that fits the design of our vacuum chamber we used the software *Radia* created for 3D magnetostatics and developed by The ESRF - European Synchrotron Radiation Facility. We used an arrangement of 8 neodymium magnets placed symmetrically around the intersection of two laser beams as shown in Fig. (14). The dimensions of the magnets are 3.2 x 12.7 x 25.4 mm and each one has a remanent magnetization of 1.3 T. A magnetic density plot in the plane xz of the magnetic field produced is shown in Fig. (15). As expected, the region which corresponds to the center of the chamber the magnetic field is zero. The magnetic field gradient is about 250 G/cm in the x direction as shown in Fig. (15).

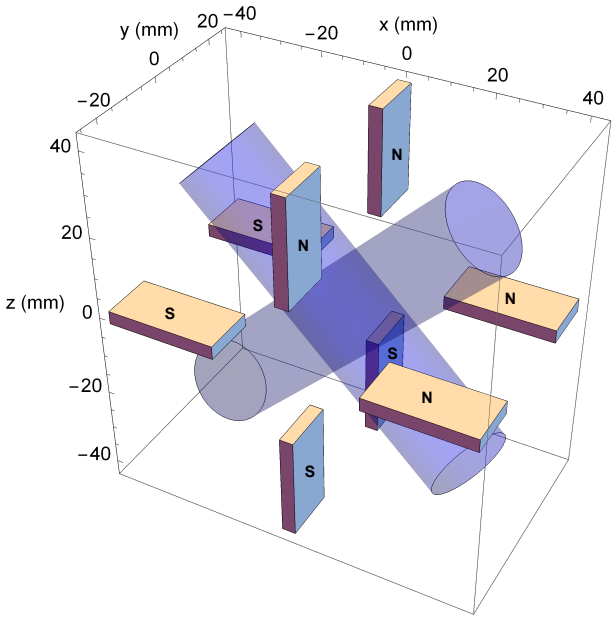

Figure 14 – Arrangement of 8 magnets around the two cooling beams for the 2D MOT setup creating a quadruple magnetic field. The centers of the magnets are separated from each other by 40 mm on the y axis, and 60 mm on the x and z axes.

Source: By the author.

With all the retroreflected beams well aligned, we managed to get a 2D MOT, as shown in Fig. (16). The 2D MOT beams have 20 mW of power and a $1/e^2$ radius of 5 mm.

3.2.3 2D MOT + "Zeeman beams"

The laser beams that make up the 2D MOT have 20 mW of power and 0.9 cm of diameter each, they are tuned 40 MHz below the strong cooling transition. Additional laser beams with 10 mW power and tuned 130 MHz below the resonance are injected counter-propagating under 45° to the atom beam ejected from the dispenser, as shown in Fig. (17). These beams are meant to have a Zeeman-like behavior to stop the atoms (but without the magnetic field gradient), capture fast atoms and increase the number of atoms in the 3D MOT.

The transition between the ground state $^1S_0$ and the first excited singlet state $^1P_1$ ($\lambda = 461$ nm, transition with $\Delta m = \pm 1$), can be used both for cooling in MOT and for slowing down atoms in the atomic beam. The relatively high transition width, $\Gamma = 2\pi \times 30.5$ MHz allows reaching high cooling rate.

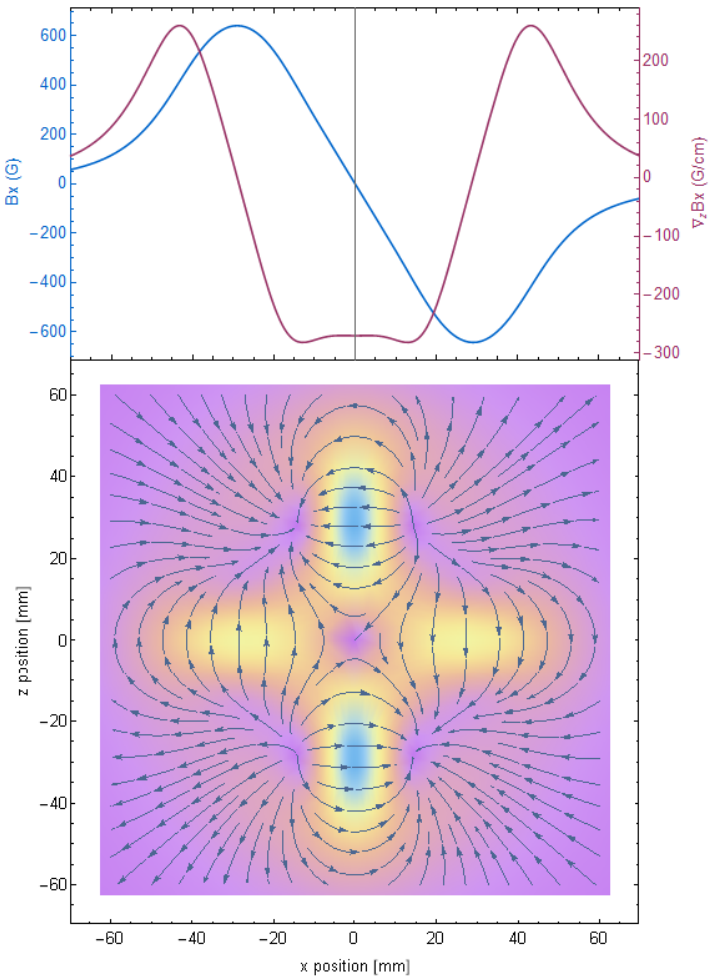

Figure 15 – Representation of the field generated by the magnets in the 2D MOT central vertical plane (y=0) orthogonal to the chamber axis. The color scale is a function of the magnitude of the field, while the vectors represent its direction. The plot on the top shows magnetic field and gradient along the central (x=y=0) vertical axis of the 2D MOT. The field along y-axis is zero.

Source: By the author.

3.3 Description of the 3D MOT setup

3.3.1 Science chamber and ring cavity

The science chamber contains in its central part an optical ring cavity (see Fig. (18b)), the cloud of atoms must be located in the center of the ring cavity to later monitor Block oscillations created by one of the counterpropagating modes of the cavity as briefly explained in Sec. (1.2). Outside the chamber, there are placed two coils to create a quadrupole magnetic field.

The blue MOT is located at the free-space waist of the ring cavity mode, where the beam diameter of the mode is 70 μm. The limited access to all viewports of the science chamber, together with the necessity to provide cooling beams from 6 directions of space

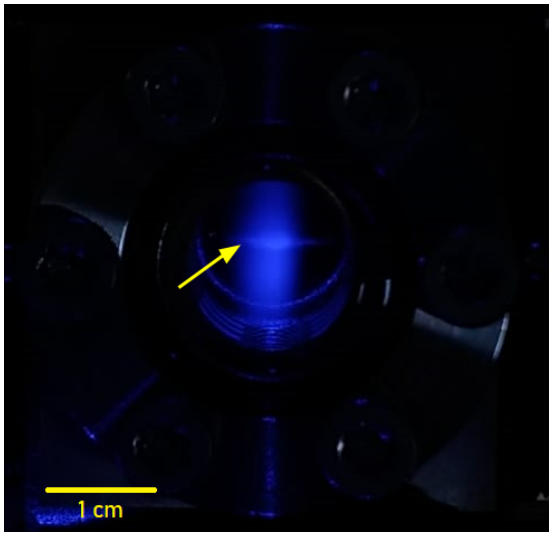

Figure 16 – Picture of 2D MOT seen from a window of the chamber. Each beam has 30 mW and the arrangement of permanent magnets creates a magnetic field gradient of 250 G/cm.

Source: By the author.

represented a challenge to get and optimize the blue MOT. Each cooling beam of the 3D MOT has approximately a $1/e^2$ radius of 4.5 mm and 3 mW of power, and each pair of counterpropagating beams has inverse circular polarization. The parameters characterizing our ring cavity are summarized in Tab. (3).

Table 3 – Summary of parameters characterizing the ring cavity.

parameter	value
cavity round trip length	L = 3.6 cm
cavity mode volume	$V = 0.5$mm
mode waist at atomic location	$w = 70$ μm
free spectral range	$\delta_{fsr} = (8.2 \pm 0.02)$ GHz
curvature of HR mirrors	$\rho = 50$ mm
reflection of the HR mirrors	$R_{hr} = 99.9$ %
reflection of the incoupler	$R_{ic} = 99.7$ %
finesse under s-polarization	$F_s \approx 1200$
finesse under p-polarization	$Fp \approx 500$
transition linewidth	$\Gamma = (2\pi)7.6$ kHz
cavity linewidth	$\kappa = (2\pi)690$ kHz
recoil shift	$\omega_{rec} = (2\pi)4.78$ kHz
coupling strength	$g_1 = (2\pi)8.7$ kHz

Source: By the author.

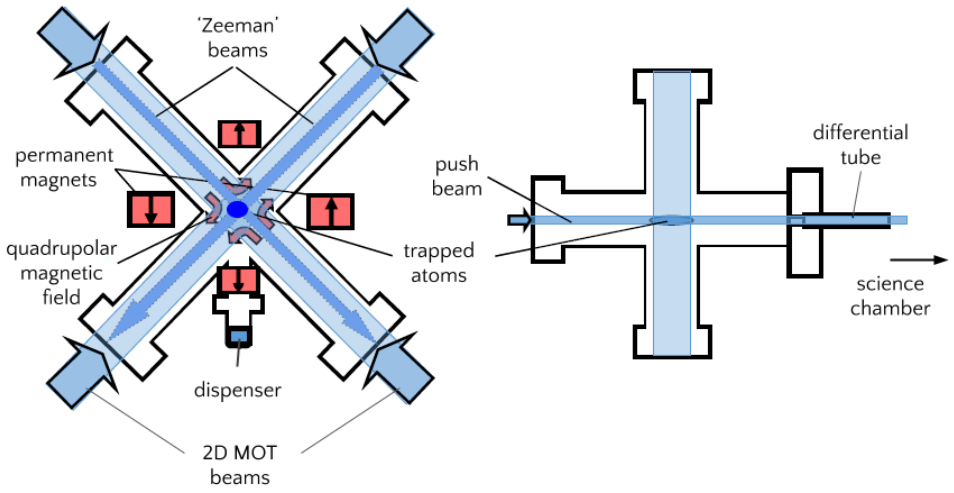

Figure 17 – Scheme of 2D MOT cooling beams joint with "Zeeman beams". The image shows the direction of propagation of the "Zeeman beams", those beams are directed from the top of the 2D MOT chamber, jointly are depicted the 2D MOT beams. In the right, is shown how a push beam carries the atoms from the 2D MOT through the differential tube toward the science chamber.

Source: By the author.

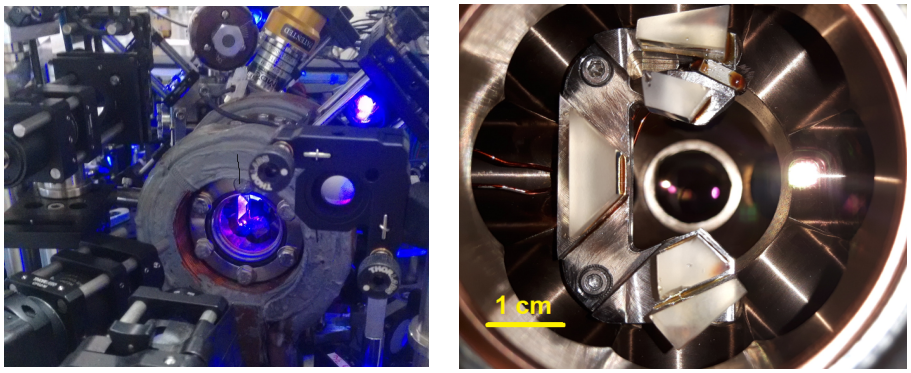

(a) (b)

Figure 18 – (a) Science chamber (b) Optical ring cavity

Source: by the author.

3.3.2 Magnetic field

The magnetic field is created by the current flowing through two coils in anti-Helmholtz configuration located at the ends of the science chamber, as it can be seen in Fig. (13). With this configuration, the central part of the ring cavity has zero magnetic field and a magnetic field gradient approximately equal to 70 G/cm, which is necessary to provide Zeeman splitting of the energy levels.

To calculate the value of the current needed to create the magnetic field, we

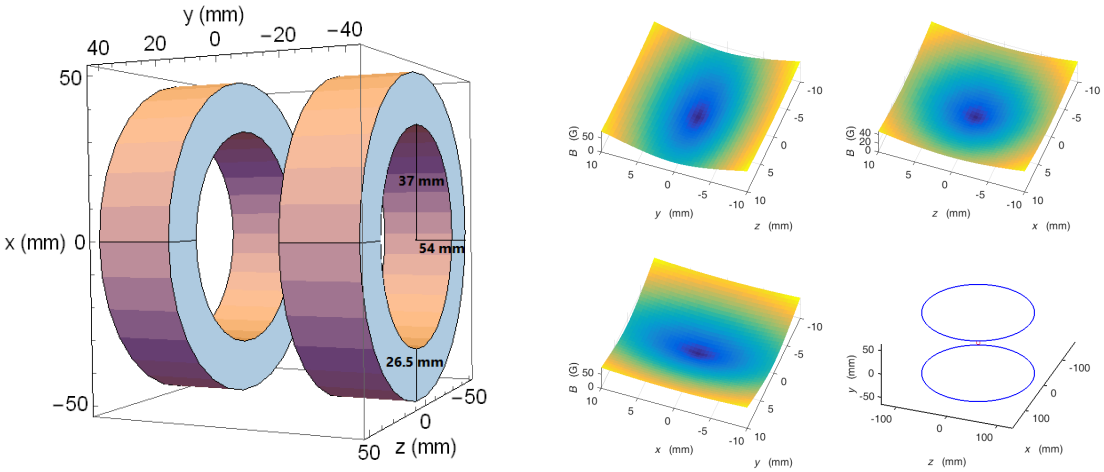

(a) (b)

Figure 19 – (a) Scheme of 3D MOT coils. (b) Magnetic field density of 3D MOT in each plane.

Source: by the author.

simulated the coils using the software *Radia*, (see Fig. (19a)). The magnetic field, produced using a pair of anti-Helmholtz coils, has a linear variation along the three axes, with the field gradient along the z axis equal to -2 times that along the x and y axes so that it satisfies $\boldsymbol{\nabla} \cdot \mathbf{B} = 0$. The pair of coils were constructed with the following specifications: a metal base with 37 mm of inner radius, 54 mm of outer radius, 26.5 mm width and 160 turns of copper wire of 1.628 mm of diameter (AWG 14), shown in Fig. (19a) .The value of the magnetic field gradient obtained is 70 G/cm and for this a current of 8.5 A. was simulated, as shown in Fig. (20).

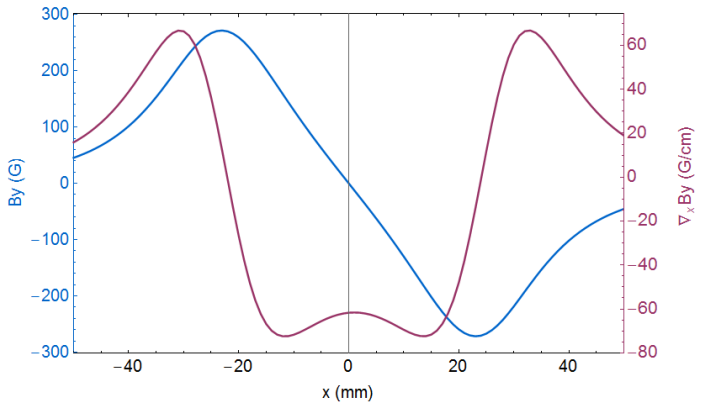

Figure 20 – Magnetic field and gradient along the y-axis with 8.5 A of current. The magnetic field gradient calculated in the simulation is 70 G/cm.

Source: By the author.

The slowed atoms were fed into a 3D MOT formed by a pair of anti-Helmholtz coils and three pairs of counterpropagating laser beams in orthogonal directions with opposite circular polarization. Each trapping beam typically has a power of 3 mW with an $1/e^2$ radius of 4.5 mm and a detuning of 45 MHz below the resonance (see Fig. (7)). This blue MOT collects 1.8×10^5 atoms approximately. As expected, this result is comparable with those obtained by other groups[43, 44] and differs by being only one order of magnitude smaller. The Fig. (21) shows a picture of the blue MOT in the science chamber.

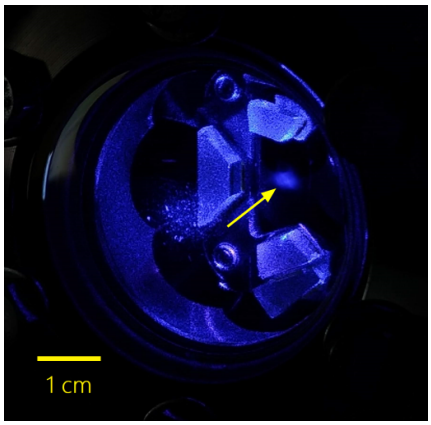

Figure 21 – Picture of the science chamber hosting a 3D MOT of strontium in the main cooling transition. The blue MOT needs to be located in the center of the ring cavity.

Source: By the author.

3.4 Imaging method

Absorption imaging is by far the most popular imaging technique used in ultracold atom experiments. It provides information about the spatial distribution of atoms, the atom number and their average temperature.[45, 46]

To apply this technique, the trap confining the atomic cloud is suddenly turned off, thus letting the atoms, accelerated by the Earth's gravitation, fall for a time of flight of a few ms. Then a pulse of a resonant laser light, whose diameter is much larger than the size of the cloud, is irradiated. The shadow printed by the atomic cloud on the transverse profile of the laser beam is recorded by a camera.

The local attenuation of the beam intensity I can be related through the absorption coefficient α (also called optical density) to the atomic density via the Beer-Lambert law $I = I_0 e^{-\alpha(x,y)}$,

$$-\ln \frac{I(x,y)}{I_0} = \alpha(x,y) = \sigma(\Delta) \int n(\mathbf{r})\, \mathrm{d}z \tag{3.4}$$

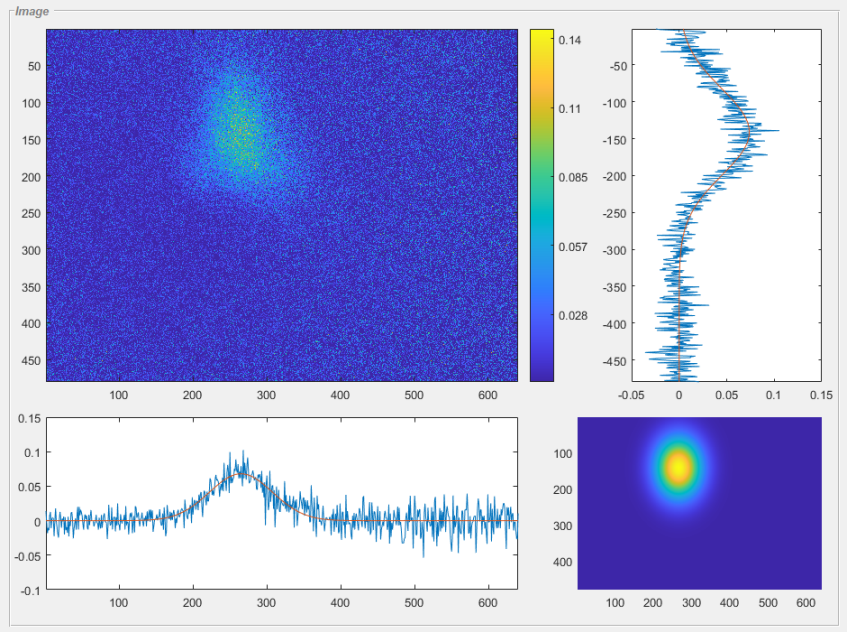

Figure 22 – Image normalized by the program in Matlab through the absorption process. Here, we represent the optical density of the blue MOT, with the corresponding gaussian fit in the vertical and horizontal axis.

Source: By the author.

where $n(\mathbf{r})$ is the density distribution of the cloud and the optical absorption cross section $\sigma(\Delta)$ is given by:

$$\sigma(\Delta) = \frac{\sigma_0}{1 + 4\left(\frac{\Delta}{\Gamma}\right)^2 + \frac{I_0}{I_{sat}}}, \tag{3.5}$$

where σ_0, is the on resonance cross section and is given by $\sigma_0 = \frac{\hbar\omega\Gamma}{2I_{sat}}$. In each experimental cycle we take three pictures: one with the probe beam illuminating completely the trapped cloud, the second only with the beams used for trapping (there are no atoms in this picture) and, the third image of the system with no laser light focusing on the region where the cloud is (in order to capture all background light). The image acquisition is done by using a National Instruments board, model PCI 6723, which controls the experiment with a minimum response time of 20 μs in the analog output. The control sequence to capture the images is detailed in Tab. (4). For each image, we associate a respective intensity: I_{Abs} the first, I_{Probe} the second and I_{Dark} for the third. A program developed in Matlab by our group then analyzes the captured images (the normalized image obtained from this software can be seen in Fig. (22)), transforming the values related to the optical density of each pixel of the image into a matrix, we can find the initial intensity I_0 normalizing the intensity I_{Probe} while we find the final intensity by normalizing I_{Abs}. With these intensities,

the optical density α is given by:

$$\alpha = -\ln \frac{I_{Abs} - I_{Dark}}{I_{Probe} - I_{Dark}}. \tag{3.6}$$

To estimate the number of atoms we rearrange the equation (3.4) and integrate along the x and y directions to get the total atom number:

$$N = \frac{1}{\sigma_0} \int_{-\infty}^{\infty} \int_{-\infty}^{\infty} \alpha(x, y) \, \mathrm{d}x\mathrm{d}y. \tag{3.7}$$

Assuming that the density distribution of the MOT is Gaussian, the density of the atom cloud is

$$n(\mathbf{r}) = n_0 \, \mathrm{e}^{-\mathbf{r}^2/2\bar{r}^2}. \tag{3.8}$$

where $\bar{r}$ is the size of the atom cloud and n_0 is the peak density. Then, the atom number can then be calculated by

$$N = \frac{2\pi\bar{r}^2\alpha(0,0)}{\sigma_0}, \tag{3.9}$$

The peak density is obtained from normalization,

$$N = \int n(\mathbf{r})\mathrm{d}^3r = n_0 \int \mathrm{e}^{-\mathbf{r}^2/2\bar{r}^2}\mathrm{d}^3r = \sqrt{2\pi}^3 n_0 \bar{r}^3 \tag{3.10}$$

$$n_0 = \frac{N}{\sqrt{2\pi}^3 \bar{r}^3} \tag{3.11}$$

The probe beam collimator and the camera are located at two opposing viewports of our science chamber. The probe beam has a $1/\mathrm{e}^2$ radius of 4.5 mm and a power of typically 40 µW, which results in a low saturation parameter $s = I/I_{sat} = 2 \times 10^{-3}$. The probe beam is controlled by turning on and off an AOM, with a rise time < 1 μs. The lens system in front of the camera has a magnification of 0.5, and each pixel of the camera chip in the atom plane corresponds to a length of 3.75 μm.

It is knows that the absorption is accompanied by radiative pressure. After some scattering events, due to the photonic recoil, the atoms have accumulated a sufficiently large velocity, and therefore a sufficiently large Doppler shift, to be out of resonance with the laser beam. Subsequent photons are no longer scattered by the atoms and only contribute to increase the illumination of the camera without carrying any information about the presence of atoms. Consequently, it is advantageous to use very short laser pulses. In addition, the intensity of the laser beam should not saturate the transition in order to guarantee an optical cross-section, which is independent of the intensity, and hence to guarantee the validity of the Beer-Lambert law. Here we did a simple estimate of what the pulse duration Δt of the probe beam should be. The momentum velocity that atoms acquire when they are illuminated by the probe beam can be expressed as

$$mv_f = \hbar k \; s\frac{\Gamma}{2} \; \Delta t, \tag{3.12}$$

where $\hbar k$ is the momentum of the photon, the product $s\frac{\Gamma}{2}$ is the decay rate of the population and Δt is the pulse duration. The Doppler shift kv_f should be less than the linewidth of the atomic resonance Γ, therefore

$$kv_f = \frac{\hbar k^2}{m}\, s\frac{\Gamma}{2}\, \Delta t < \Gamma \tag{3.13}$$

$$\frac{\hbar k^2}{2m}\, s\Delta t < 1, \tag{3.14}$$

Replacing the recoil shift $\omega_{rec} = \hbar k^2/2m$ (for the 461 nm transition $\omega_{rec} = 134$ kHz),

$$\Delta t < \frac{1}{\omega_{rec} s} \approx 2 \text{ ms} \tag{3.15}$$

the pulse duration must not be grater than 2 ms. In our case, we set the pulse the shorter we could, it was 0.02 ms.

3.4.1 Imaging setup

The imaging system we use for this experiment is composed of two lenses (Fig. 23) located outside the vacuum chamber.
Lens 1 (objective): Thorlabs AC254-100-A-ML (f = 100 mm); Lens 2 (eyepice): Thorlabs AC254-050-A-ML (f = 50 mm); Point Gray Chameleon CMLN-1352M CCD camera with a quantum efficiency of 46% at 461 nm. The system was designed to give a demagnification of 0.45, and the pixel size is of 3.75 x 3.75 μm^2.

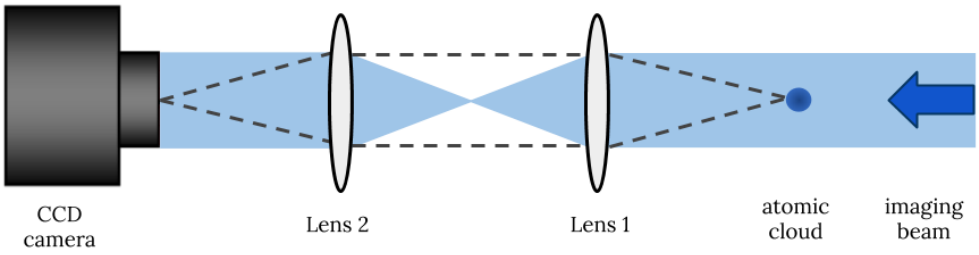

Figure 23 – Schematic of the absorption imaging system used in the experiment. The atom cloud is illuminated by a probe beam which is resonant with it. The absorption of light by the atoms casts a shadow which is then imaged onto a CCD camera. The lens array creates an image demagnification of 0.45.

Source: By the author.

3.5 Dependencies of blue MOT on the push beam

Once the atoms are pre-cooled and trapped in the 2D MOT, a push beam transfers the atoms to the science chamber. This beam has a 1/e^2 radius of 1.1 mm and is sent

Table 4 – Summary of the sequence of the experiment for absorption imaging.

Sequence	Time	Description
Loading time	5 s	All cooling beams and magnetic field are on.
Time of flight	0.2 ms	Magnetic field and push beam off.
Arm CCD	0.04 ms	The camera is prepared to receive the trigger, all cooling beams and magnetic field off.
Probe pulse (with atoms)	0.02 ms	At this point there is still a cloud of atoms despite the beams and the magnetic field being turned off. The probe light is absorbed by the cloud and the camera records a "shadow" of the atoms.
Wait exposure	40 ms	Time for the camera to record the image.
Wait read out	100 ms	Time to take the image to the computer through a data acquisition board.
Arm CCD	0.04 ms	The camera is prepared to receive the second trigger.
Probe pulse (without atoms)	0.04 ms	The camera captures the probe light without atom cloud.
Wait exposure	40 ms	Time for the camera to record the second image.
Wait read out	100 ms	Time to take the second image to the computer through a acquisition board.
Arm CCD	0.04 ms	Camera is prepared to receive the third trigger.
Capture background (dark)	0.04 ms	The camera captures the backgroud in the third image.
Wait exposure	40 ms	Time for the camera to record the third image.
Wait read out	100 ms	Time to take the third image to the computer through a acquisition board.

Source: By the author.

from a transverse window of the 2D MOT chamber pushing the atoms to the center of the ring cavity (see Fig. (13)). It is quite difficult to properly align this beam, as it has to pass through a 2 mm diameter tube which connects the two chambers to maintain the difference of pressure.

In the transfer of atoms from the 2D MOT, the atoms have to travel a distance of approximately 20 cm, which corresponds to the separation between the centers of the two chambers. So, it was necessary to consider the fall of atoms by the action of gravity. For this we perform a simple estimation as explained below.

The force exerted by the push beam is given by,

$$F = \hbar k \Gamma_p \tag{3.16}$$

where the scattering rate is

$$\Gamma_p = \frac{6\pi}{k^2} \frac{\Gamma^2}{4\Delta^2 + 2\Omega^2 + \Gamma^2} \frac{I_p}{\hbar\omega}. \tag{3.17}$$

If the push beam is on resonance, but the atom is moving with velocity v, then $\Delta = kv$. If the push beam is week, $\Omega \approx 0$. We obtain a differential equation,

$$F(v) = m\dot{v} = \hbar k \frac{6\pi}{k^2} \frac{\Gamma^2}{4k^2v^2 + \Gamma^2} \frac{I_p}{\hbar\omega} = \frac{6\pi I_p}{ck^2} \frac{\Gamma^2}{4k^2v^2 + \Gamma^2}. \tag{3.18}$$

It can be solved by,

$$\int_0^{v_0} (4k^2v^2 + \Gamma^2) dv = \int_0^{t_0} \frac{6\pi I_p \Gamma^2}{2cmk^2} \mathrm{d}t, \tag{3.19}$$

that is,

$$v_0^3 + \frac{3\Gamma^2}{4k^2} v_0 = \frac{9\pi I_p \Gamma^2}{2cmk^4} t_0. \tag{3.20}$$

Setting $P_p = 130\mu$W and $w_0 = 1.1$ mm, we get with $I_p = \frac{2P_p}{\pi w_0^2}$ the following curves in Fig. (24) for the position s of the atoms and their velocity v as a function of time. For comparison the figures also show a curve with $P_p = 30\mu$W and the transfer due to thermal motion of the atoms along the horizontal axis:

$$v_{thermal} = \sqrt{\frac{k_B T}{m}}. \tag{3.21}$$

The gravitational sag the atom will suffer during the transfer time is,

$$z_{sag} = \frac{g}{2} t^2. \tag{3.22}$$

Fig. (24) demonstrates that, without push beam, the gravitational sag is way too large, and the transfer to the science chamber is not possible.

Fig. (24a-c) shows the position, instantaneous velocity and acceleration of the atoms along the optical axis. The greater the power of the push beam, the less time the atoms need to reach the science chamber and the sag would be negligible. The opposite happens if the power decreases, the sag of the atoms increases, as seen in Fig. (24d). However, if the power of the push beam is too high, the atoms may exceed the capture velocity of the MOT, which would prevent trapping the atoms.

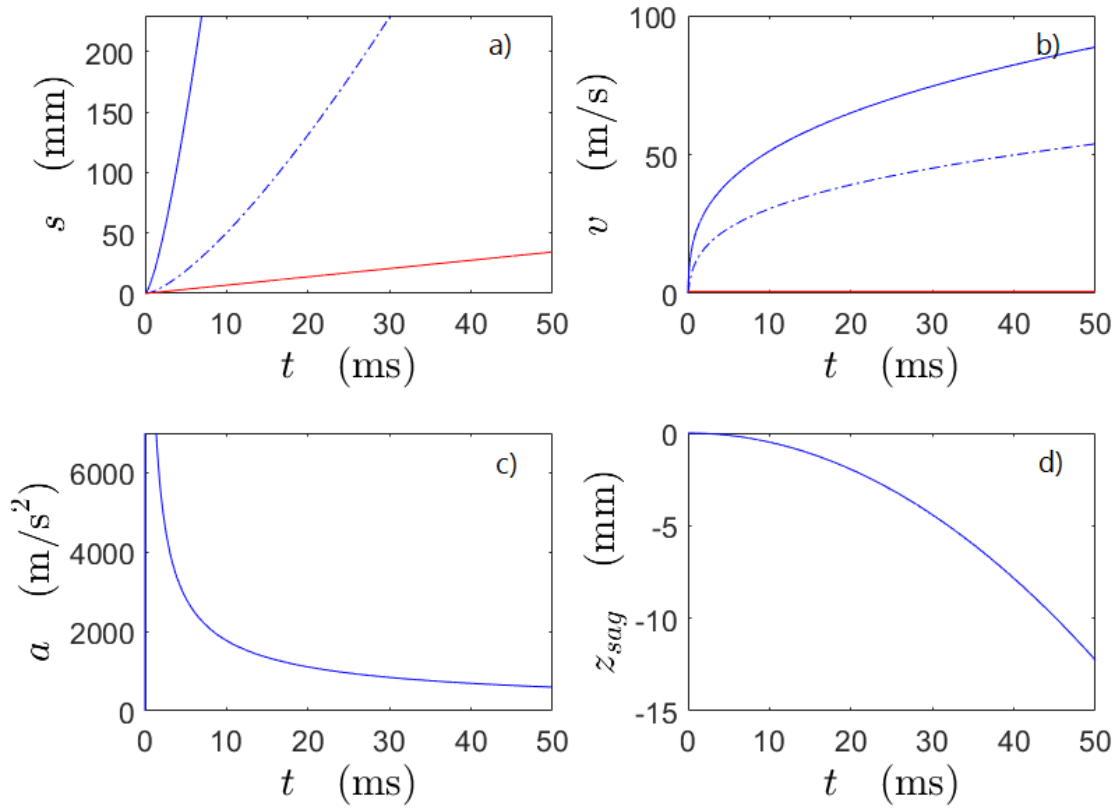

Figure 24 – (a-c) Position, instantaneous velocity, and acceleration along the optical axis. Blue solid curves: push beam transfer with $P_p = 130$ μW. Blue dash-dotted curves: push beam transfer with $P_p = 30$ μW. Red solid curves: thermal atoms transfer with $P_p = 0$. (d) Gravitational sag perpendicular to the optical axis.

Source: By the author.

In order to find the optimum power of the push beam, we did several loading rate measurements of the blue MOT by changing the push beam power between 30μW (0.04 I_{sat}) and 130μW (0.164 I_{sat}) –in the $^1S_0 \rightarrow ^1P_1$ transition of strontium, the saturation intensity is $I_{sat} = 43$ mW/cm^2–,[47] out of this range of power it was not possible to perform a reliable measurement due to the very low optical density of the blue MOT. In Fig. (25a), the measurements for 0.04, 0.076 and 0.164 times I_{sat} are shown. The data is fitted by the function $N(t) = R\tau\left(1 - e^{t/\tau}\right)$, where R is the loading rate and τ is the lifetime. The summarized results of blue MOT loading rate as a function of the pushing beam intensity I_p are shown in Fig. (25b). The loading rate reaches a peak at push beam intensities around $I_p = 0.09 I_{sat}$, beyond which it decreases rapidly as I_p becomes larger. Larger push beam intensities lead to a better collimation of the atomic beam, but also to too high velocities such that the atoms can not be captured anymore.

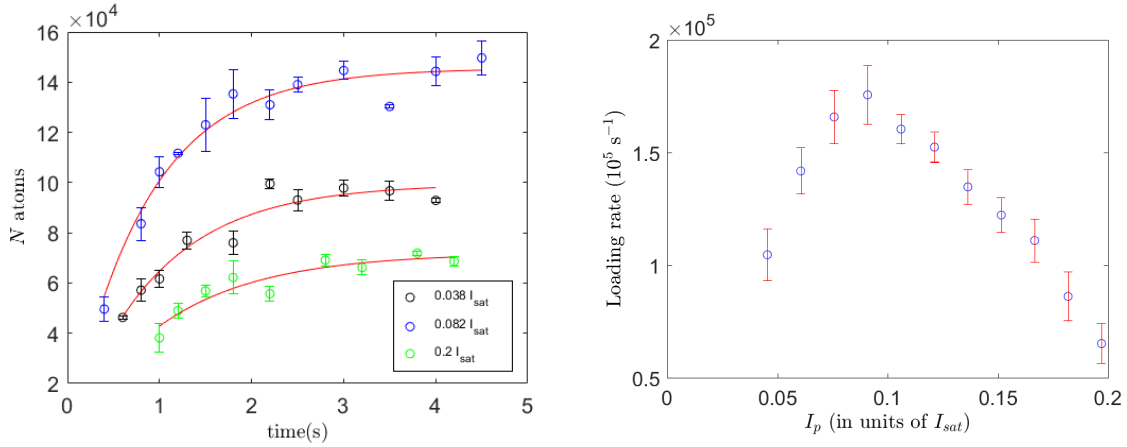

Figure 25 – Loading rate of the blue MOT measurement by changing the push beam intensity. (a) Number of atoms versus loading time with 0.02, 0.04 and 0.08 times the saturation intensity (b) Loading rate versus intensity of the push beam. The loading rate reaches a peak at push beam intensities around $I_p = 0.09 I_{sat}$, beyond this intensity, it decreases rapidly.

Source: by the author.

3.6 Dependencies of blue MOT on 2D MOT and "Zeeman" beams

The number of atoms in the blue MOT as a function of the intensity of the 2D MOT beams I_{2D} is shown in Fig. (26a). It rises monotonically with increasing I_{2D} until a threshold value of about 75 mW/cm^2, while at larger intensities it begins to saturate.

Once the 2D MOT parameters are optimized together with the push beam, we align the beams we named "Zeeman" designed to trap the fastest atoms that are emitted from the dispenser, as discussed in Sec. (3.2.3). To be able to see a greater effect of the Zeeman beams, it was necessary to redistribute the blue light power that we had available, that is, we decreased the power of the 2D MOT beams and rest was used for the Zeeman beams. We measured the number of atoms in the blue MOT as a function of the Zeeman beams power and the results are shown in Fig. (26b). The number of atoms increases monotonously as the power of the Zeeman beams increases. Without Zeeman beams, the maximum number of atoms reached was 1.65×10^5 (see Fig. (26a)), while with Zeeman beams, the number of atoms increased to 2.2×10^5 approximately, which represents in our case, an increase of 20 %. In addition, it can be seen in Fig. (26b) that with our maximum available power (26 mW/cm^2) a saturation level has not yet been reached.

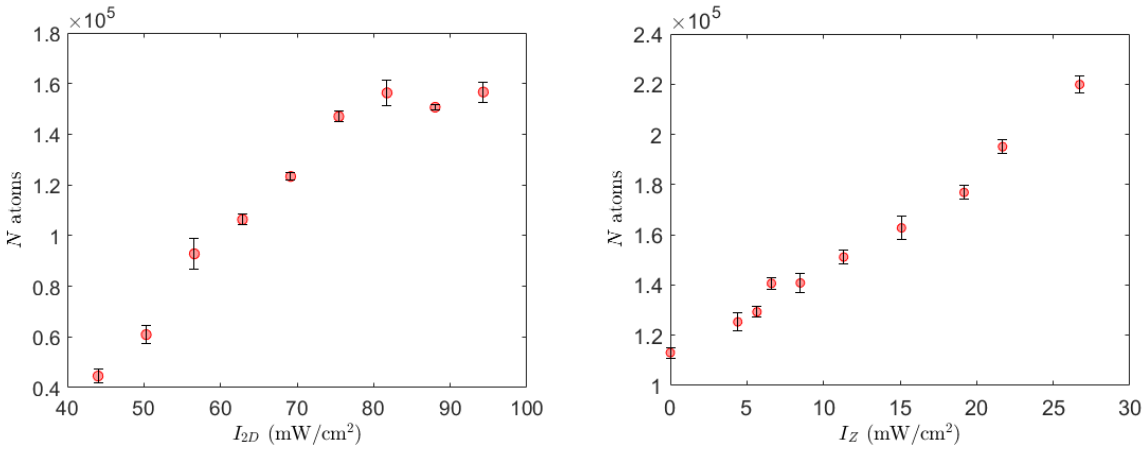

Figure 26 – (a) Number of atoms of blue MOT versus 2D MOT beams intensity. The number of atoms rises until it begins to saturate at $I_{2D} \approx 75$ mW/cm^2 (b) Number of atoms of blue MOT versus Zeeman beams power. The number of atoms increases monotonously as the power of the Zeeman beams increases. Using Zeeman beams, the number of atoms increased to 2.2×10^5 approximately, which represents an increase of 20% of the atom number.

Source: by the author.

3.7 Repumping

The main cooling transition of strontium is not fully closed, as described in Sec. (1.3). Atoms can decay into a metastable state, limiting the atom numbers of the MOT. At least one repumping laser is required, that recycles the population of atoms pumped into the metastable state $(5s5p)^3P_2$, and eventually a second repumper laser that recycles the atoms pumped into the metastable $5s5p^3P_0$ (in which some atoms fall after being repumped from the $^3P_2$). We use two commercial *Toptica* lasers of 707 nm and 679 nm corresponding to $^3P_2 \rightarrow ^3S_1$ and $^3P_0 \rightarrow ^3S_1$ respectively, see Fig. (2).

Maximum powers of 15.5 mW and 5.3 mW are available for the laser of 707 nm and 679 nm respectively, both have a $1/e^2$ radius of 4 mm approximately. These lasers can operate without being stabilized to an external reference, but their frequency will need to be readjusted after 30-40 minutes.

In our experiment, it is very difficult to directly observe a blue MOT without using the repump light, it is even almost imperceptible to the CCD camera used in the imaging system. So it is worth emphasizing that all the measures presented in this thesis include the influence of the two repump beams.As explained in Sec. (2.2.1), in accordance with results obtained by other groups,[32, 21] the estimated lifetime of the blue MOT without repump light is 20 ms. With the repump light, the 1/e lifetime we measured assuming an exponential decay is 0.84 s.

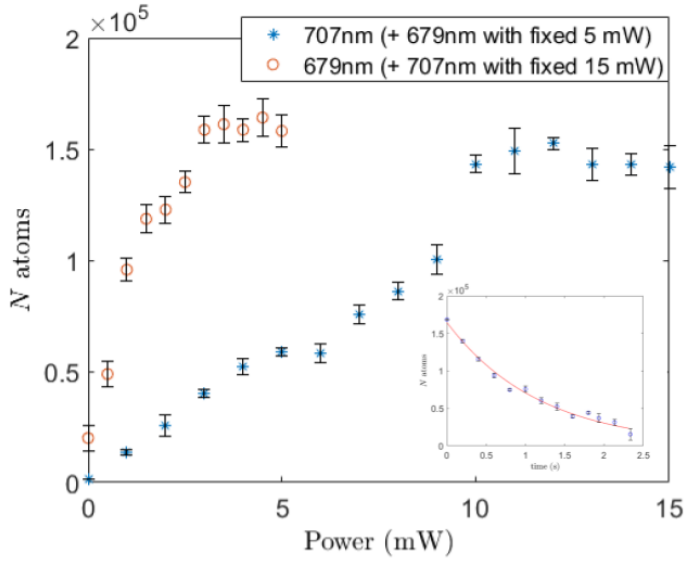

Figure 27 – Number of atoms of blue MOT versus the power of the repump beams. In order to capture absorption images it is necessary that both lasers act on the MOT. Blue (red) marks shows the increase in the number of atoms by increasing the laser power of 707 nm (679 nm) and keeping the maximum laser power of 679 nm (707 nm) fixed. The results show that to reach the maximum number of atoms it is enough to use 5 mW and 10 mW of the 679nm and 707 nm lasers respectively. The inset plot shows the lifetime measurement using repump light, considering an exponential decay $N(t) = N_0 e^{(-t/\tau)}$, the blue MOT lifetime increased to $\tau = 0.84$ s.

Source: By the author.

Fig. (27) shows the number of atoms of the blue MOT versus the power of the repump beams. We can see that is enough to use 10 mW (5 mW) of 707 nm (679 nm) laser to reach the maximum number of trapped atoms (1.6×10^5). In our case, if only the laser of 707 nm acts on the blue MOT, the number of atoms does not increase significantly, that is, in order to observe a strong repumping effect, it is necessary to use the two lasers together.

3.8 Dependency of blue MOT on the magnetic field

As explained in Sec. (3.3.2), the magnetic field gradient required to obtain our 3D MOT is 70 G/cm, this is achieved with a pair of coils in anti-Helmholtz configuration with a current of 9 A. This gradient is responsible for keeping the cloud of atoms imprisoned at the point of zero magnetic field. An image of the cloud's optical density is shown in Fig. (28) by varying the value of the magnetic field gradient. In this case, it can be seen that if the magnetic field gradient is lower than 70 G/cm, the cloud of atoms is more expanded and it can be seen that the optical density is low. As the gradient increases, the density of the cloud begins to increase and it shifts slightly upwards. This happens because the cloud

is centered at the zero point of the magnetic field, otherwise, by varying the magnetic field gradient, the cloud would expand unevenly. In our case it is important to verify that the atom cloud is at the zero point of the magnetic field in order to make the transfer to the red MOT. For this is necessary to vary the magnetic field gradient from 70 G/cm to approximately 7 G/cm and during this switching time, the cloud is sensitive to the action of gravity. In addition, it is important to our experiment that the final position of the cloud be at the center of the ring cavity. To ensure that this is accomplished, in the future it may be necessary to use compensation coils in order to overcome the displacement of the cloud.[22]

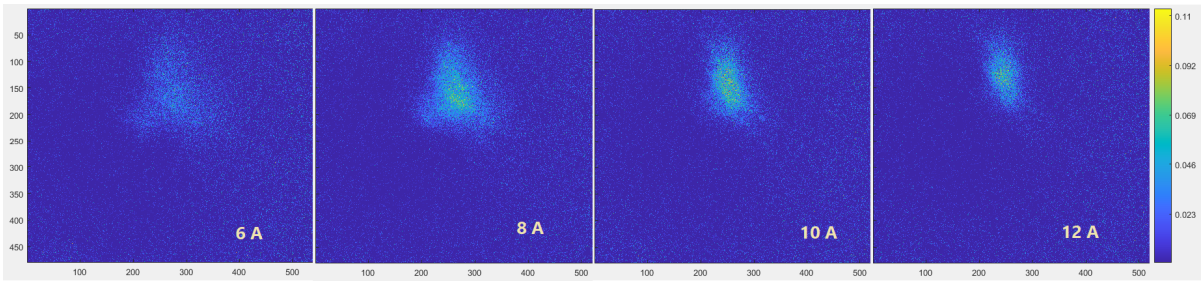

Figure 28 – Absorption imaging pictures of the optical density of blue MOT obtained by varying the current of the coils: 6, 8, 10 and 12 A, corresponding to a magnetic field of 46.7, 62.2, 77.8, 93.3 G/cm respectively. The optical density of the atom cloud increases when the magnetic field gradient is greater than 70 G/cm and it even moves slightly upwards.

Source: By the author.

For our experiment it is important to optimize the number of atoms. Therefore, by varying the magnetic field current of the 3D MOT, we see that the number of atoms reaches a maximum value at 8.5 A (66 G/cm) and decreases rapidly with lower or greater currents (Fig. (29a)). In addition, the optical density reaches a maximum value between 8 and 10 A, as seen in Fig. (29b).

3.9 Temperature measurement

The temperature of the cold atomic sample is one of its most important characteristics and several methods have been proposed and used for its determination. Most of them take advantage of the thermal expansion of the sample after its release from the trap.[48] These time-of flight (TOF) measurements are performed by acquiring the absorption signal of the probe laser beam through the falling and expanding atomic cloud.

The density distribution of an atomic cloud with temperature T after a time of flight t_{tof} is $n(\mathbf{r}) = n_0 \mathrm{e}^{-\mathbf{p}^2/2mk_BT}$ with $\mathbf{p} = \frac{m\mathbf{r}}{t_{tof}}$.

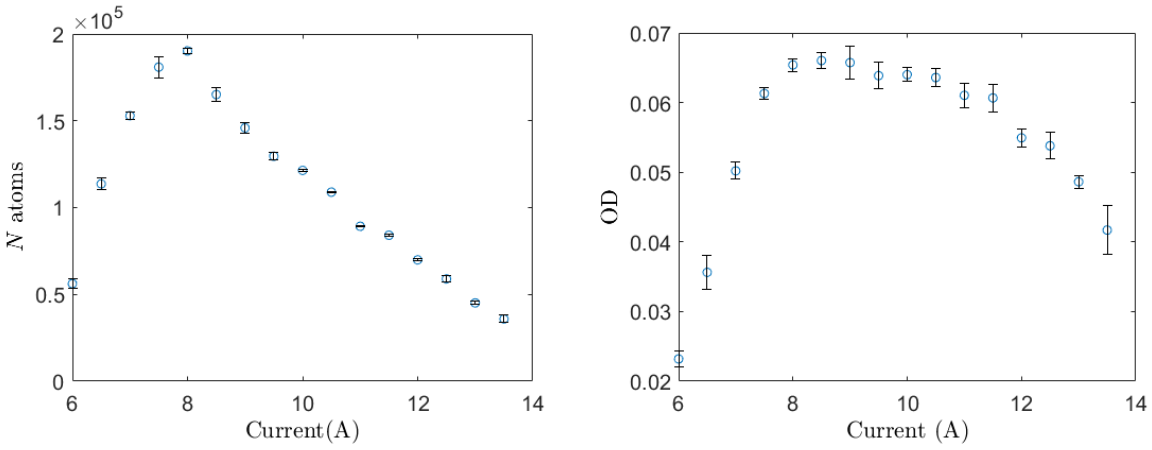

(a) (b)

Figure 29 – (a) Number of atoms of blue MOT versus magnetic field current, the maximum number of atoms is reached with 8.5 A (66 G/cm), with lower or greater currents the number of atoms decreases rapidly. (b) The optical density of blue MOT reaches a maximum value between 8 and 10 A.

Source: by the author.

Defining the size of the trapped cloud as $\bar{r} \equiv t_{tof}\sqrt{\frac{k_B T}{m}}$ we get

$$n(\mathbf{r}) = n_0 \mathrm{e}^{-\mathbf{r}^2/2\bar{r}^2}. \tag{3.23}$$

And the temperature is given by:

$$T = \frac{m}{kB}\left(\frac{\bar{r}}{t_{tof}}\right)^2 \tag{3.24}$$

The cooling beams are extinguished by switching off the AOM and by a mechanical shutter. The originally trapped atoms expand for a variable time t_{tof}, after which their shadow is imaged on a camera. The magnetic field gradient is kept off during the atom expansion and then is sent the imaging pulse. To the measured MOT size two Gaussians are fitted, with standard deviations $\bar{r}_x$ and $\bar{r}_y$ corresponding to the horizontal and vertical dimensions. The squares of these standard deviations are then plotted over the squared time, as shown in Fig. (30). To the experimental data we then fit the formula $\bar{r}^2 = \bar{r_0}^2 + \frac{k_B T}{m} t_{tof}^2$, with the mass of strontium $m = 88$ u, and with the fitting parameters being the temperature T and the mean square velocity $\bar{r}_0^2/t_{tof}^2 = \langle v^2 \rangle$. The resulting temperature is 4.6±0.3 mK for the x axis and 3.5±0.3 mK for the y axis. The reason for the different temperatures along the two axes is not completely clear, but we consider that it depends on the initial shape of the cloud which actually is not uniformly circular. The approximate value of a few mK is in agreement with reported values of other groups.[49, 37] The initial radius of the atom cloud in the x axis is $\bar{r}_{0x}$ =0.23±0.03 mm and in the y axis $\bar{r}_{0y}$ =0.31±0.03 mm. The resulting mean velocity $\bar{v} = \sqrt{\langle v^2 \rangle}$ is $\bar{v}_x$ =65.9±0.3 cm/s and $\bar{v}_y$ =58.2±0.3 cm/s.

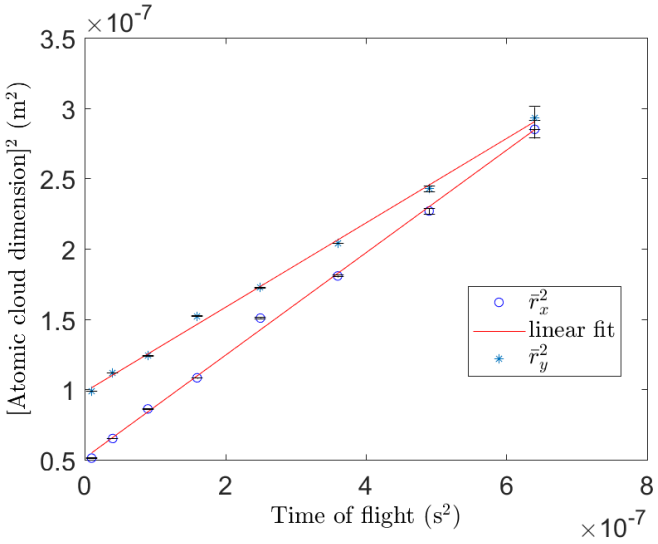

Figure 30 – Time of flight measurement. The squares of the MOT sizes (Gaussian standard deviations) along two directions are plotted versus the squared time-of-flight with both the cooling beams and magnetic field off. The fitted equation is $\bar{r}^2 = \bar{r_0}^2 + \frac{k_B T}{m} t_{tof}^2$, resulting a temperature of 4.6 mK in the x axis and 3.5 mK in the y axis.

Source: By the author.

3.9.1 Summary

This chapter detailed the characteristics and properties of the blue MOT and all the parameters necessary to optimize the number of atoms, temperature, size, etc. The following table (5) summarizes the power, beam size and detuning values of each of the components of the blue system, and also includes the final values of the number of atoms, temperature, cloud size, lifetime and loading rate.

Table 5 – Summary of the optical parameters of the blue system.

Saturation spectroscopy	beams power $1/e^2$ radius detuning $\omega_l - \omega_0$	probe: 3 mW, pump: 7 mW 2.1 ± 0.1 mm (-)130 MHz
2D MOT	beams power $1/e^2$ radius detuning $\omega_l - \omega_0$	24 mW 5.0 ± 0.2 mm 33 MHz (red detuned)
Push beam	power $1/e^2$ radius detuning $\omega_l - \omega_0$	70 μW 2.2 ± 0.1 mm 10 MHz (blue detuned)
3D MOT	beams power $1/e^2$ radius detuning $\omega_l - \omega_0$	4 mW 4.5 ± 0.2 mm 30 MHz (red detuned)
	magnetic field gradient	66 G/cm coils current: 8.5 A
Imaging beam	power $1/e^2$ radius detuning $\omega_l - \omega_0$	30 μW 4.5 ± 0.2 mm resonant
Repump beams	beams power	679 nm: 5 mW 707 nm: 15 mW
	frequency	679 nm: 441.33245 THz 707 nm: 423.91326 THz
Blue MOT	number of atoms	N=2×10^5
	temperature	$T_x = 4.6 \pm 0.3$ mK $T_y = 3.5 \pm 0.3$ mK
	cloud size	$\bar{r}_{0x}$ =0.23±0.03 mm $\bar{r}_{0y}$ =0.31±0.03 mm
	1/e lifetime	0.84 s
	loading rate	1.8 $\times10^5$ s^{-1}

Source: By the author.

4 OUTLOOK

4.1 Red MOT of strontium

For the implementation of the idea of a continuous monitoring in atomic interferometry, two main ingredients based on different physical phenomena are necessary: the first is the Bloch oscillations and the second is the concept of Collective Atomic Recoil Laser, CARL. As explained in Sec. (1.2), Bloch oscillations are an effect where particles behave like matter wave and are subjected to quantum regime. Therefore, the atomic motion can no longer be described by the classical equations and must be quantized. CARL is observed with atoms interacting with the two counterpropagating modes of an annular optical cavity, due to the conversion of kinetic energy of the atoms used for the creation of a laser radiation field containing information about atomic motion. The created field serves as a non-destructive and continuous proof of the dynamics of the matter wave and of the inertial forces to which it is subjected.

In order for a cloud of atoms to behave as quantum waves instead of classical particles, it must reach ultra-cold temperatures, that is, the cloud must be cooled to temperatures below the recoil limit $T_{recoil} = \hbar^2 k^2 / 2mk_B$, typically on the order of few μK. The recoil temperature is equal to the recoil energy deposited in a single atom initially at rest by the spontaneous emission of a single photon, and represents a lower limit for the temperature which can be reached with some laser cooling techniques.

The presence of narrow intercombination lines in strontium offers the opportunity to add a second cooling stage after the blue MOT in order to reach ultra-cold temperatures and increase the density of the ensemble. This prevents us from using other cooling methods like the evaporative cooling, which usually comes with important loses in the number of atoms.

Generally, the atoms are pre-cooled in a MOT operated on the blue cooling transition, before being transferred to a red MOT operated on the narrow intercombination line the $^1\mathrm{S}_0 - ^3\mathrm{P}_1$ at 689 nm. The magnetic field gradients are switched within 200 μs from 70 G/cm to 7 G/cm. For this, we need to switch the current in the anti-Helmholtz coils generating the magnetic fields from 9 A to 0.5 A. This is done via a snubber circuit with 47 μF of capacitance and 100 Ω of resistance. At the time of the transfer from the blue to the red MOT the atomic cloud has a temperature around 5 mK, which corresponds to a Doppler broadening of 7 MHz at the frequency of the intercombination line. This is much larger than the linewidth of the intercombination line, which reduces the spectral overlap with the red MOT laser. In order to cool all atoms, we frequency modulate the red MOT laser with a 30 kHz modulation frequency and a modulation excursion, which

starts at 5 MHz and is gradually reduced to 0 as the cloud cools down.[50] This cooling stage works using a more elaborated red laser spectrometer and locking scheme, which will be described in detailed in a future work.

To sum up, the lasers operating near the 689 nm intercombination line have three tasks: (1) cool the atoms close to recoil temperature, (2) generate the vertical standing wave along the ring cavity axis, in which the strontium atoms shall perform Bloch oscillations, and (3) inject a probe light into the ring cavity measuring the motional state of the matter wave.

Currently the project is in this second stage of atom cooling, we have not yet obtained the red MOT, but we are confident that in the near future we can expand the obtained results so far and continue to report the new advances of the project.

5 CONCLUSIONS

This thesis describes the experimental setup and procedure for the generation of ultra-cold strontium atoms which will be used in the future to study a method of continuous monitoring of Bloch oscillations in an optical ring cavity.

On a broader view, strontium offers attractive potential for laser cooled experiments, benefiting from its versatile level structure, whilst the easily accessible wavelength allows for assembly of simpler and more compact setups. The atomic structure of strontium allows for two main cooling transitions. One is the $^1\mathrm{S}_0 - ^1\mathrm{P}_1$ and the corresponding wavelength is 461 nm with a broad linewidth of $\Gamma/2\pi = 30.5$ MHz. This transition is well-suited for traditional laser cooling, permitting a thermal beam of dilute strontium gas to be cooled to mK temperatures and collected in a MOT. The second main cooling transition is particularly interesting because of its very fine intercombination, the transition $^1\mathrm{S}_0 - ^3\mathrm{P}_1$ of $\Gamma/2\pi = 7.6$ kHz linewidth in 689 nm. The greatest advantage of this fine transition lies in the fact that it allows to reach ultra low temperatures by purely optical cooling, we avoid to apply evaporative cooling methods, which traditionally are slow and always come with important losses in the number of atoms. This will allow the investigation of the interaction of the atoms with the ring cavity in the quantum regime.

The experimental setup comprises the ultra-high vacuum system in which the experiments take place. It was designed with a two chamber concept, allowing for efficient loading and offering a science chamber with low pressure and shielding for black body radiation from the strontium source. The lasers addressing the broad cooling transition of strontium are frequency-stabilized by a saturated absorption spectroscopy system, whose creation, assembly and operation was described in detail.

Once the two chambers were properly installed and the coils were working, we started the assembly of the optical instruments to prepare the cooling, push and imaging beams. Then, we reached the stage of obtaining the optical magneto traps. In a short time we got the 2D MOT. However, it took more time to get the 3D MOT and stabilize the system to be able to characterize it. In part this was due to the malfunction of the Ti:Sapphire laser, which forced us to stop the experiment several times and led us to change the way of distribution of the beams in order to work with the low power we had available. Other reasons were the high sensitivity of the blue MOT to the alignment, power and frequency of the push beam, in addition the nature of the experiment required that the 3D MOT be aligned vertically, so it was always quite complicated to align the six beams of the 3D MOT and the control of the polarization was also somewhat difficult.

We managed to obtain a blue MOT that trapped 2.2×10^5 atoms, at an average temperature of 4 mK. The properties of the cold atomic beam are particularly sensitive to the pushing beam intensity. ^{88}Sr MOT loading rates exceeding 10^5 s^{-1} are achieved in our setup and a lifetime of 0.84 s.

One innovative component of the setup is a 2D MOT for strontium atoms. It minimizes black-body radiation and vacuum contamination at the position of the final experiment, and also, the 2D MOT can be mounted in a much more compact way. This represents a great advantage compared to the use of a Zeeman slower. In addition, our 2D MOT has two additional beams tuned in resonance which reach the cloud of atoms from the upper viewports of the chamber. These beams we called "Zeeman", due to their function of slow down the fastest atoms emitted from the dispenser, similar to what a Zeeman slower would do. The implementation of these beams allowed us to increase the number of atoms in the 3D MOT by 20 %. This percentage could increase a little more if we had more laser power available.

In conclusion, we now have a platform prepared to begin the second stage of cooling atoms. The current conditions of temperature, position, number of atoms and density of the atomic cloud are optimal for doing the transfer to a MOT in the intercombination line of 689 nm and 7.6 kHz. Being able to reach this point has been very challenging because of all the technical inconveniences that appeared along the way. However, now the blue system is fully characterized and stabilized in order to continue with the project. With the implementation of the second stage red MOT in the near future, the atoms will be cooled enough to interact with the two modes of the ring cavity and will be possible to study the monitoring of Bloch oscillations through the CARL phenomenon.

REFERENCES

1 NABIGHIAN, M.; ANDER, M.; GRAUCH, V.; HANSEN, R.; LAFEHR, T.; LI, Y.; PEARSON, W.; PEIRCE, J.; PHILLIPS, J.; RUDER, M. Historical development of the gravity method in exploration. **Geophysics**, v. 70, n. 6, p. 63–89, 2005.

2 LAFEHR, T. Gravity method. **Geophysics**, v. 46, n. 11, p. 1634–1639, 1980.

3 WICHT, A.; HENSLEY, J.; SARAJLIC, E.; CHU, S. A preliminary measurement of the fine structure constant based on atom interferometry. **Physica Scripta**, T102, n. 1, p. 82–88, 2002.

4 STUHLER, J.; FATTORI, M.; PETELSKI, T.; TINO, G. M. MAGIA – using atom interferometry to determine the newtonian gravitational constant. **Journal of Optics B:** quantum and semiclassical optics, v. 5, n. 2, p. 75–81, 2003.

5 MILTON, K. The Casimir effect: recent controversies and progress. **Journal of Physics A:** mathematical and general, v. 37, n. 38, p. 209–277, 2004.

6 ANTEZZA, M.; PITAEVSKII, L.; STRINGARI, S. New asymptotic behavior of the surface-atom force out of thermal equilibrium. **Physical Review Letters**, v. 95, n. 11, p. 113202, 2005.

7 FERRARI, G.; POLI, N.; SORRETINO, F.; TINO, G. M. Long-lived Bloch oscillations with bosonic Sr atoms and application to gravity measurement at the micrometer scale. **Physical Review Letters**, v. 97, n. 6, p. 060402, 2006.

8 IDO, T.; ISOYA, Y.; KATORI, H. Optical-dipole trapping of Sr atoms at a high phase-space density. **Physical Review A**, v. 61, n. 6, p. 061403, 2000.

9 MICKELSON, P.; ESCOBAR, Y. Martinez de; YAN, M.; DESALVO, B.; KILLIAN, T. C. Bose-Einstein condensation of ^{88}Sr through sympathetic cooling with ^{87}Sr. **Physical Review A**, v. 81, n. 5, p. 051601, 2010.

10 PEDEN, B.; MEISER, D.; CHIOFALO, M.; HOLLAND, M. Nondestructive cavity QED probe of Bloch oscillations in a gas of ultracold atoms. **Physical Review A**, v. 80, n. 4, p. 043803, 2009.

11 VENKATESH, B. P.; TRUPKE, M.; HINDS, E.; O'DELL, D. Atomic Bloch-Zener oscillations for sensitive force measurements in a cavity. **Physical Review A**, v. 80, n. 6, p. 063834, 2009.

12 DAHAN, M.; PEIK, E.; REICHEL, J.; CASTIN, Y.; SALOMON, C. Bloch oscillations of atoms in an optical potential. **Physical Review Letters**, v. 76, n. 24, p. 4508–4511, 1996.

13 KRUSE, D.; CUBE, C. von; ZIMMERMANN, C.; COURTEILLE, P. W. Observation of lasing mediated by collective atomic recoil. **Physical Review Letters**, v. 91, n. 18, p. 183601, 2003.

14 BLACK, A.; CHAN, H.; VULETIC, V. Observation of collective friction forces due to spatial self-organization of atoms: from Rayleigh to Bragg scattering. **Physical Review Letters**, v. 91, n. 20, p. 203001, 2003.

15 SLAMA, S.; BUX, S.; KRENZ, G.; ZIMMERMANN, C.; COURTEILLE, P. W. Superradiant rayleigh scattering and collective atomic recoil lasing in a ring cavity. **Physical Review Letters**, v. 98, n. 5, p. 053603, 2007.

16 BUX, S.; GNAHM, C.; MAIER, R.; ZIMMERMANN, C.; COURTEILLE, P. Cavity-controlled collective scattering at the recoil limit. **Physical Review Letters**, v. 106, n. 20, p. 203601, 2011.

17 CLADÉ, P.; GUELLATI-KHÉLIFA, S.; SCHWOB, C.; NEZ, F.; JULIEN, L.; BIRABEN, F. A promising method for the measurement of the local acceleration of gravity using Bloch oscillations of ultracold atoms in a vertical standing wave. **Europhysics Letters**, v. 71, n. 5, p. 730–736, 2005.

18 POLI, N.; WANG, F.; TARALLO, M.; ALBERTI, A.; PREVEDELLI, M.; TINO, G. M. Precision measurement of gravity with cold atoms in an optical lattice and comparison with a classical gravimeter. **Physical Review Letters**, v. 106, n. 3, p. 038501, 2011.

19 SAMOYLOVA, M.; PIOVELLA, N.; HUNTER, D.; ROBB, G. R. M.; BACHELARD, R.; COURTEILLE, P. W. Mode-locked Bloch oscillations in a ring cavity. **Laser Physics Letters**, v. 11, n. 12, p. 126005, 2014.

20 SAMOYLOVA, M.; PIOVELLA, N.; ROBB, G. R. M.; BACHELARD, R.; COURTEILLE, P. W. Synchronization of Bloch oscillations by a ring cavity. **Optics Express**, v. 23, n. 11, p. 14823–14835, 2015.

21 SORRETINO, F.; FERRARI, G.; POLI, N.; DRULLINGER, R.; TINO, G. M. Laser cooling and trapping of atomic strontium for ultracold atom physics. **Modern Physics Letters B**, v. 20, n. 21, p. 1287–1320, 2006.

22 STELLMER, S. **Degenerate quantum gases of strontium**. 2013. 246 p. Ph.D Thesis (Doctor of Science) – Faculty of Mathematics, Computer Science and Physics, University of Innsbruck, Innsbruck, 2013. Available from: http://www.ultracold.at/theses/2013-stellmer.pdf. Accessible at: 10 Nov. 2018.

23 CHIN, C.; GRIMM, R.; JULIENNE, P. S.; TIESINGA, E. Feshbach resonances in ultracold gases. **Reviews of Modern Physics**, v. 82, n. 2, p. 1225–1286, 2010.

24 WANG, Y. B.; ; YIN, M. J.; REN, J.; XU, Q. F.; LU, B. Q.; HAN, J. X.; GUO, Y.; CHANG, H. Strontium optical lattice clock at the National Time Service Center. **Chinese Physics B**, v. 27, n. 2, p. 023701, 2018.

25 POLI, N.; SCHIOPPO, M.; VOGT, S.; FALKE, S.; STERR, U.; LISDAT, C.; TINO, G. M. A transportable strontium optical lattice clock. **Applied Physics B**, v. 117, n. 4, p. 1107–1116, 2014.

26 KOCK, O.; HE, W.; SWIERAD, D.; SMITH, L.; HUGHES, J.; BONGS, K.; SINGH, Y. Laser controlled atom source for optical clocks. **Scientific Reports**, v. 6, p. 37312, 2016.

27 BARKER, D. **Degenerate gases of strontium for studies of quantum magnetism**. 2016. 172 p. Ph.D Thesis (Doctor of Philosophy) – Department of Physics, University of Maryland, College Park, 2016. Available from: https://drum.lib.umd.edu/handle/1903/18617. Accessible at: 1 Jul. 2019.

28 POLI, N.; DRULLINGER, R.; FERRARI, G.; LEONARD, J.; SORRENTINO, F.; TINO, G. M. Cooling and trapping of ultracold strontium isotopic mixtures. **Physical Review A**, v. 71, n. 6, p. 061403, 2005.

29 DALIBARD, J.; COHEN-TANNOUDJI, C. Dressed-atom approach to atomic motion in laser light: The dipole force revisited. **Journal of the Optical Society of America B**, v. 2, n. 11, p. 1707–1720, 1985.

30 RAND, S. C. **Lectures on light**: nonlinear and quantum optics using the density matrix. New York: Oxford University Press, 2010. 304 p.

31 METCALF, H. **Laser cooling and trapping**. New York: Springer, 2002. 323 p.

32 XU, X.; LOFTUS, T. H.; HALL, J. L.; GALLAGHER, A.; YE, J. Cooling and trapping of atomic strontium. **Journal of the Optical Society of America B**, v. 20, n. 5, p. 968–976, 2003.

33 BOYD, M. **High precision spectroscopy of strontium in an optical lattice: towards a new standard for frequency and time**. 2007. 223 p. Ph.D Thesis (Doctor of Philosophy) – Department of Physics, University of Colorado, Boulder, 2007. Available from: https://jila.colorado.edu/yelabs/sites/default/files/uploads/theses_2007_08_martyboyd.pdf. Accessible at: 1 Sept. 2018.

34 DEMTRÖDER, W. **Laser spectroscopy**. Berlin: Springer, 1973.

35 NATARAJAN, V. **Modern Atomic Physics**. Boca Raton: CRC Press, 2015.

36 LIDE, D. R. **CRC Handbook of chemistry and physics**. 86th edition. Boca Raton: CRC Press/ Taylor & Francis, 2006. 4-130 p.

37 WANG, S.; WANG, Q.; LIN, Y.; WANG, M.; LIN, B.; ZANG, E. Cooling and trapping ^{88}sr atoms with 461 nm laser. **Chinese Physics Letters**, v. 26, n. 9, p. 093202, 2009.

38 KOCK, B. O. **Magneto-optical trapping of strontium for use as a mobile frequency reference.** 2013. 177 p. Ph.D Thesis (Doctor of Philosophy) – College of Engineering and Physical Sciences, University of Birmingham, Birmingham, 2013. Available from: https://etheses.bham.ac.uk/id/eprint/4635. Accessible at: 10 Sept. 2018.

39 YANG, T.; PANDEY, K.; PRAMOD, M.; LEROUX, F.; KWONG, C.; HAJIYEV, E.; CHIA, Z.; FANG, B.; WILKOWSKI, D. A high flux source of strontium atoms. **The European Physical Journal D**, v. 69, n. 10, p. 1–12, 2015.

40 LUDLOW, D.; ZELEVINSKY, T.; CAMPBELL, G. K.; BLATT, S.; BOYD, M. M.; MIRANDA, M. de; MARTIN, M. J.; THOMSEN, J. W.; FOREMAN, S. M.; YE J. FORTIER, T. M.; STALNAKER, J. E.; DIDDAMS S. LE COQ, Y.; BARBER, Z. W.; POLI, N.; LEMKE, N. D.; BECK, K. M.; OATES, C. W. Sr lattice clock at 1 x 10^{-16} fractional uncertainty by remote optical evaluation with a Ca clock. **Science**, v. 139, n. 5871, p. 1805–1808, 2008.

41 BARBIERO, M.; TARALLO, M.; CALONICO, D.; LEVI, F.; LAMPORESI G. FERRARI, G. Sideband-enhanced cold atomic source for optical clocks. **Physical Review Applied**, v. 13, n. 1, p. 014013, 2020.

42 TIECKE, T. G.; GENSEMER, S. D.; LUDEWIG, A.; WALRAVEN, J. T. M. High-flux two-dimensional magneto-optical-trap source for cold lithium atoms. **Physical Review A**, v. 80, n. 1, p. 013409, 2009.

43 HU, F.; NOSSKE, I.; COUTURIER, L.; CANZHU, T.; QIAO, C.; CHEN, P.; JIANG, Y. H.; ZHU, B.; WEIDEMULLER, M. Analyzing a single-laser repumping scheme for efficient loading of a strontium magneto-optical trap. **Physical Review A**, v. 99, n. 3, p. 033422, 2019.

44 MORIYA, P. H.; ARAÚJO, M. O.; AO, F. T.; HEMMERLING, M.; KESSLER, H.; SHIOZAKI, R.; TEIXEIRA, R.; COURTEILLE, P. W. Comparison between 403 nm and 497 nm repumping schemes for strontium magneto-optical traps. **Journal of Physics Communications**, v. 2, n. 12, p. 125008, 2018.

45 WANG, Y.; HU, Z. H.; QI, L. Comparison of two absorption imaging methods to detect cold atoms in magnetic trap. **Chinese Physics B**, v. 24, n. 2, p. 024203, 2015.

46 SMITH, D.; AIGNER, S.; HOFFERBERTH, S.; GRING, M.; ANDERSSON, M.; WILDERMUTH, S.; KRÜGER, P.; SCHNEIDER, S.; SCHUMM, T.; SCHMIEDMAYER, J. Absorption imaging of ultracold atoms on atom chips. **Optics Express**, v. 19, n. 9, p. 8471–8485, 2011.

47 JAVAUX, C.; HUGHES, I.; LOCHEADA, G.; MILLEN, J.; M.P.A., J. Modulation-free pump-probe spectroscopy of strontium atoms. **European Physical Journal D**, v. 57, n. 2, p. 151–154, 2010.

48 KETTERLE, W.; DURFEE, D. S.; STAMPER-KURN, D. M. Making, probing and understanding Bose-Einstein condensates. *In:* INGUSCIO, M.; STRINGARI, S.; WIEMAN, C.E. (ed.). **Bose-Einstein condensation in atomic gases.** Amsterdam: IOS Press, 1999. p. 67-176. (Proceedings of the International School of Physics "Enrico Fermi", v. 140).

49 NOSSKE, I. **Cooling and trapping of strontium atoms for quantum simulation using Rydberg states**. 2018. 109 p. Ph.D Thesis (Doctor of Philosophy) – University of Science and Technology of China, Shanghai, 2018. Available from: http://quantum.ustc.edu.cn/rydberg/files/nosske2018.pdf. Accessible at: 8 May. 2018.

50 KATORI, H.; IDO, T.; ISOYA, Y.; KUWATA-GONOKAMI, M. Magneto-optical trapping and cooling of strontium atoms down to the photon recoil temperature. **Physical Review Letters**, v. 82, n. 6, p. 1116–1119, 1999.